Tracking the dynamics of systems evolving through infrequent transitions in a network of discrete states

Doros N. Theodorou, Nikolaos Lempesis, George C. Boulougouris

National Technical University of Athens,
School of Chemical Engineering
9 Heroon Polytechniou Street, Zografou Campus
157 80 Athens, Greece
E-mail: doros@chemeng.ntua.gr

Many physicochemical, materials, and biological systems whose dynamics is too slow to be addressed via conventional molecular dynamics (MD) simulations can be considered as evolving in time through infrequent transitions in a network of discrete states, each state providing a coarse-grained description of a domain in multidimensional configuration space. We briefly discuss how states can be defined starting from the detailed potential energy hypersurface of such a system and how rate constants for transitions between states can be estimated based on the theory of infrequent events. We then concentrate on tracking the evolution of a system as a succession of transitions between states. Two general approaches are introduced for this: Kinetic Monte Carlo simulation, and analytical solution of the master equation for the time-dependent probabilities of occupancy of the states. For the latter approach we outline how time autocorrelation functions can be computed under equilibrium and nonequilibrium conditions. We present examples from the computation of diffusivities of gases in zeolites and in glassy amorphous polymers. We then introduce the method of Dynamic Integration of a Markovian Web (DIMW), designed to track relaxation towards equilibrium from a narrow initial distribution among states by solving the master equation in a network of explored states that is progressively augmented on the fly. We present an application of the DIMW method to physical ageing in a glassy polymer. Finally, we outline how computation of the long-time evolution in a network of states can be simplified by "lumping" states into clusters of states.

1 Introduction

The dynamics of many physical, chemical, materials, and biological systems is slow because it proceeds as a succession of infrequent transitions between domains in their configuration space, which we shall call "states". The states constitute "basins" of low potential energy with respect to the generalized coordinates spanning configuration space, or of low free energy with respect to a set of order parameters providing a coarse-grained description of the system. Each state contains one or more local minima of the the free energy. Transitions between states are infrequent events, in the sense that the mean waiting time for transition out of a state is long in comparison to the time required for the system to establish a restricted equilibrium distribution among configurations in the state. The entire configuration space can be tessellated into states. Representing each state in a coarse-grained sense by a point in configuration or in order parameter space and connecting all pairs of states hetween which a transition is possible, one obtains a graph, or network of states. Examples of phenomena that can be modelled as occurring through a succession of transitions in a network of states include diffusion of defects and impurities in metals and semiconductors;[1] of gas molecules in amorphous polymers;[2] of bulky hydrocarbons in microporous solids, such as zeolites;[3] structural relaxation and plastic deformation in

glasses;[4] phase transitions in molecular and atomic clusters;[5] surface diffusion;[6] protein folding[7]; and chemical reactions.[8]

The possibility of coarse-graining dynamics into a sequence of transitions in a network of states is of strategic importance for understanding and predicting macroscopic time-dependent properties from atomic-level structure and interactions. The longest times that can be simulated with atomistic MD on conventional computational means are microseconds. (Note, however, that millisecond-long MD runs on specialized hardware have been reported recently.[9]) This is too short by many orders of magnitude in comparison with the experimental time scales of most phenomena of interest. A more efficient strategy than "brute-force" MD is to construct a network of states i and compute the rate constants $k_{i \to j}$ between them from atomic-level information. By definition, the rate constant $k_{i \to j}$ is a conditional probability per unit time that a transition to state j will occur, provided the system is in state i.

Once states and interstate rate constants are known, the system evolution at the state level can be tracked by solving the master equation:

$$\frac{\partial P_i(t)}{\partial t} = \sum_{j \neq i} P_j(t) k_{j \to i} - P_i(t) \sum_{j \neq i} k_{i \to j} \text{ , or } \frac{\partial \mathbf{P}(t)}{\partial t} = \mathbf{K}\mathbf{P}(t) \tag{1}$$

The transition rate constant $k_{i \to j}$ is independent of time, thanks to the time scale separation which makes the transition an infrequent event.[10,11] The evolution of the system in state space is a Poisson process.[12] $P_i(t)$ is the probability of occupancy of state i at time t. According to Eq.(1) this changes as a result of influx of probability from other states and efflux of probability to other states. State occupancy probabilities are normalized over all n states of the system. The time-dependent vector $\mathbf{P}$ in the matrix representation of Eq.(1) has all the $P_i(t)$ as elements. The $n \times n$ rate constant matrix is defined by $K_{ij} = k_{j \to i}$, $K_{ii} = -\sum_{j \neq i} k_{i \to j}$. At very long times, the system will adopt its equilibrium probability distribution among states, $\mathbf{P}(\infty)$. This is a stationary solution of the master equation, Eq.(1), by virtue of the condition of microscopic reversibility satisfied by the rate constants:

$$k_{i \to j} P_i(\infty) = k_{j \to i} P_j(\infty) \tag{2}$$

These notes address the problem of how to solve the master equation, Eq. (1), and learn about the long-time dynamics of a system evolving through a succession of infrequent transitions between discrete states. Sections 2 and 3 briefly discuss how states can be identified and rate constants for transitions between states can be computed, given the potential energy as a function of atomic coordinates and the masses of all atoms in the system. Section 4 reviews the basics of Kinetic Monte Carlo (KMC) simulation for generating stochastic trajectories consisting of long successions of jumps between states. Section 5 outlines a method for analytical solution of the master equation and computation of time autocorrelation functions therefrom. Example applications of the KMC and master equation solution strategies to diffusion problems are presented in sections 6 (for xenon in the zeolite silicalite) and 7 (for CO_2 in a glassy poly(amide imide)). Section 8 addresses the more complex problem of nonequilibrium relaxation of a system that is initially confined to a small subset of states. States are not known a priori, but have to be charted out as the system relaxes. We introduce the "Dynamic Integration of a Markovian Web" (DIMW) method for solving the master equation in a network of states that is progressively augmented "on the fly". We apply DIMW to the very challenging problem of tracking struc-

tural relaxation in a polymer glass. Finally, in section 9 we discuss a systematic approach for "lumping" groups of states that communicate with each other through relatively fast transitions into single "metastates" and thereby reducing the number of states needed for the description of dynamics at long times.

2   Identifying States

States are regions of configuration space where the system is trapped for long periods of time. Let f be the number of degrees of freedom needed to specify the microscopic configuration of a system. For a classical system of N particles with periodic boundary conditions described in full detail, $f = 3N - 3$. We will use the f-dimensional vector $\mathbf{r}$ to denote the configuration of a system. We will also use $\mathbf{x}$ to denote the f-dimensional vector of mass-weighted coordinates, with elements $m_l^{1/2} r_l^\alpha$ with m_l being the mass of particle l ($l = 1, 2, \ldots, N$) and r_l^α being the position coordinate of particle l along direction α ($\alpha = 1, 2, 3$). Let $\mathcal{V}(\mathbf{x})$ be the potential energy of the system as a function of the mass-weighted coordinates. A state is a domain in $\mathbf{x}$-space surrounding a local minimum of $\mathcal{V}(\mathbf{x})$.

For small f, an exhaustive determination of all minima and consequent identification of all states and dividing surfaces between them is possible. For example, in the case of low-occupancy diffusion of a monatomic sorbate in a zeolite represented as a rigid framework,[13] $f = 3$ (the three translational degrees of freedom of the sorbate within the rigid zeolite). The volume of the asymmetric unit of the zeolite unit cell was discretized into voxels of edge length approximately 0.2 Å. A steepest descent trajectory was initiated at the center of each voxel, terminating in a local minimum of $\mathcal{V}(\mathbf{x})$. The minimization was refined using a quasi-Newton algorithm. In this way, a "drainage pattern" was constructed in three-dimensional space, leading to the local minima. The set of all voxels from which the steepest descent construction terminated at a certain minimum was assigned to the state of that minimum. Similarly, the dividing surface between two states i and j was defined as the set of all faces (squares) shared by two voxels such that the steepest descent construction from one of the voxels leads to minimum i, while that from the other voxel leads to minimum j. An exhaustive identification of all states was simularly undertaken in the work of Snurr et al.[14] on the diffusion of benzene in the zeolite silicalite, where both the zeolite framework and the sorbate molecule were represented as rigid. In this case, $f = 6$ degrees of freedom (three translational and three orientational of the benzene relative to the framework) come into play. A very large number of insertions of the benzene at random positions and orientations within the asymmetric unit was used as a first step. From each configuration resulting from insertion that did not exceed a certain energy threshold, a quasi-Newton minimization was initiated, leading to an energy minimum in $\mathcal{V}(\mathbf{x})$ in six-dimensional configuration space, representing a sorption state. Increasing the number of random insertions for the initial guess configuration did not lead to any other minima; this, and the symmetry of determined minima, indicated that the calculation was exhaustive.

In more complex situations, where f is larger, the identification of states can be greatly facilitated by geometric analysis. An example is provided by Greenfield's study of methane diffusion in glassy atactic polypropylene.[15] Static configurations of the amorphous polymer, constituting local minima of its potential energy, were used as a starting point. Within each static configuration, the volume accessible to spherical probes of various radii smaller

than the van der Waals radius of the penetrant of interest (methane) was analyzed using a Delaunay tessellation and clustering algorithm.[16] For large probe radius the accessible volume consists of relatively small disjoint clusters. As the probe radius decreases, accessible volume clusters grow in size and some clusters merge at narrow "necks" of accessible volume. The position of each of these necks between a pair of clusters is used as an initial guess for the position of the penetrant at the saddle point of the energy along the transition from a (meta)state of occupancy of one cluster to a (meta)state of occupancy of the other. A saddle point of $\mathcal{V}(\mathbf{x})$ is computed from the geometrically obtained neck position as follows: The center of the penetrant is placed at the neck position and a saddle point is first calculated with respect to the three translational degrees of freedom of the penetrant, keeping the configuration of the polymer fixed. Using this three-dimensional saddle point as an initial guess, the number of system degrees of freedom with respect to which the saddle point is calculated is progressively increased, by including more and more atoms of the polymer in concentric spheres around the penetrant. This calculation goes on until the saddle point energy becomes asymptotic with respect to inclusion of additional polymer degrees of freedom.[15] The saddle point searches can be performed using the Cerjan-Miller type algorithm of Baker.[17] Having obtained a multidimensional saddle point in both penetrant and matrix degrees of freedom, an entire transition path is constructed using Fukui's intrinsic reaction coordinate approach:[18] Starting at the saddle point, the system is displaced by a small step along the eigenvector corresponding to the negative eigenvalue of the Hessian matrix of second derivatives $\partial \mathcal{V}/(\partial \mathbf{x} \partial \mathbf{x}^{\mathrm{T}})$. Subsequently, a steepest descent construction in $\mathcal{V}(\mathbf{x})$ is undertaken using small steps in $\mathbf{x}$, until a local minimum of $\mathcal{V}(\mathbf{x})$ is reached. Completing this construction on either side of the saddle point, i.e. with the initial displacement first along the positive and then along the negative direction of the eigenvector, yields an entire reaction path between two (meta)states, in which different adjacent clusters of accessible volume are occupied by the penetrant. This calculation has been extended by Vergadou to more complex multiatom penetrants, such as CO_2 in a poly(amide imide) (see Figure 1).[19]

When no guidance is provided by geometry or crystal symmetry, the identification of states is considerably more involved. Kopsias[20] and Boulougouris[21] addressed the problem of finding connected minima in the full configuration space ($f = 3N - 3$) in order to track structural relaxation in a glass. Given a minimum of $\mathcal{V}(\mathbf{x})$, they strove to find as many as possible other minima connected to it via transition paths passing through a single first-order saddle point of $\mathcal{V}(\mathbf{x})$. For this purpose, they undertook saddle point searches in f-dimensional space, starting off along the lowest-curvature eigendirections of the Hessian at the original minimum. Beyond a certain number of searches, no new saddle points were located (the algorithm returned saddle points that had already been found); this was taken as an indication that all relevant transitions out of the initial minimum (i.e., transitions taking the system over reasonably low energy barriers), had been found. In Ref. 20 the saddle point searches were conducted using the Baker algorithm, while Ref. 21 employed the dimer method of Henkelman and Jónsson, which does not require second derivatives.[22] From each saddle point located in this way, a pair of steepest descent constructions was undertaken in full configuration space using Fukui's intrinsic reaction coordinate approach, as described above. On one side the original minimum was recovered, while on the other side the steepest descent construction led to a new minimum adjacent to the original one. The procedure was repeated from each new minimum, in order to map out a network of

$r_P = 1.28\text{Å}$ $r_P = 1.1\text{Å}$
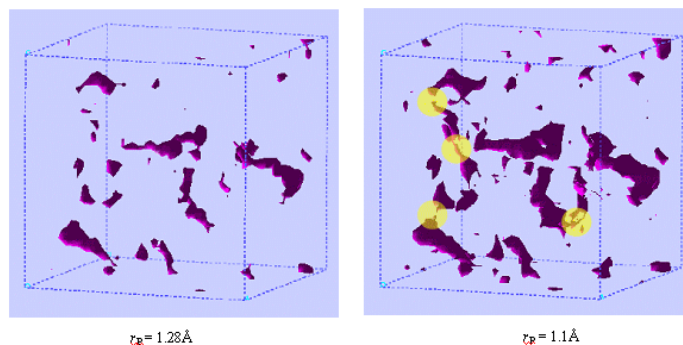
Figure 1. Geometric analysis of accessible volume in an amorphous poly(amide imide) configuration aimed at the identification of states and transition paths for diffusion of CO_2 at infinite dilution within the polymer. Analysis with a spherical probe of radius $r_P = 1.28$ Å reveals disjoint. elongated clusters of accessible volume. Analysis with a smaller probe radius $r_P = 1.1$ Å reveals "necks" of accessible volume connecting the original clusters. The positions of the necks (encircled in the figure) are used as initial guesses for the center of mass position of the penetrant at the saddle point along an elementary transition path.

minima, or "states".

In many problems it is a good approximation to assume that the reaction coordinate taking the system from a state to another state is shaped by a relatively small subset of "primary" degrees of freedom, the remaining degrees of freedom fluctuating rapidly and achieving a constrained equilibrium distribution subject to the values of the primary set. Then, system "states" can be defined as local minima of the *potential of mean force* with respect to the primary subset of degrees of freedom. Although calculating the potential of mean force is generally a challenge for molecular simulations, the reduction of dimensionality in passing from the full configuration space to the subspace of primary degrees of freedom greatly facilitates the definition of states and transitions between them. An example of such an approach based on the potential of mean force is provided by Forester and Smith's[23] calculations on the diffusion of benzene in silicalite. These authors used a unidimensional reaction coordinate, corresponding to the projection of the center of mass position of the sorbed benzene on the axes of straight or sinusoidal channel segments in the zeolite. The latter axes were taken as rectilinear, for simplicity. All other degrees of freedom (translational of the benzene in directions transverse to the channel axis, orientational of the benzene, and vibrational of the surrounding zeolite framework) were integrated over at each position along an axis. The potential of mean force was computed by dragging the benzene along the channels, through the "blue moon ensemble" MD method. States were readily identified as local minima of the potential of mean force (see also section 3).

3 Calculating Rate Constants

Once states have been defined, the transition rate constants $k_{i \to j}$ can be computed by a variety of methods. We briefly outline some of these methods here. For a more thorough treatment, the reader is referred to standard texts on molecular simulation.[24]

If transitions are subject to relatively low barriers (say, up to 7 $k_B T$), such that rate constants $k_{i \to j}$ are relatively high (say, up to ns^{-1}), then rate constants can be estimated by MD simulation. All one needs is a technique to map every configuration recorded in the course of a MD trajectory onto a state. Very often, when states are defined as regions around local minima in configuration space, this mapping is accomplished by direct energy minimization leading to the closest energy minimum or "inherent structure". [25] A reduced trajectory of states visited is thus accumulated in parallel with the MD trajectory. Switches between states can readily be identified along this reduced trajectory. Rate constants can be computed by statistical analysis of the reduced trajectory, capitalizing on the exponential distribution of waiting times that characterizes Poisson processes. A simple method that can be used for this purpose is "hazard plot analysis", outlined in the following paragraphs.[26]

We first introduce some definitions that are generally applicable to any stochastic process involving infrequent transitions. The particular example of stochastic process we will have in mind is that of exiting a specific state i in the network of states we have introduced in section 1, once the system has entered that state. The rate constant for this process is $k_{i \to} = \sum_{j \neq i} k_{i \to j}$. For the stochastic process considered, let $\hat{P}(t)$ be the probability of having undergone a transition at time t. In our particular example, $\hat{P}(t)$ can be interpreted as the cumulative distribution function of residence (or "waiting") times within state i. The hazard rate, $\hat{h}(t)$, is defined such that $\hat{h}(t)dt$ equals the (conditional) probability that a system (in an ensemble of systems governed by the stochastic process) which has not undergone a transition until time t, will undergo a transition at time t. From the definitions of $\hat{P}(t)$ and $\hat{h}(t)$, the following differential equation is satisfied:

$$\hat{P}(t + dt) = \hat{P}(t) + \left[1 - \hat{P}(t) \right] \hat{h}(t) dt \tag{3}$$

or

$$d\hat{P}/dt = \left[1 - \hat{P}(t) \right] \hat{h}(t) \tag{4}$$

Eq. (4) must be solved with initial condition $\hat{P}(0) = 0$. The solution is

$$\hat{P}(t) = 1 - \exp \left[- \int_0^t \hat{h}(t')dt' = \right] = 1 - \exp \left[-\hat{H}(t) \right] \tag{5}$$

where we have defined the cumulative hazard $\hat{H}(t)$ as

$$\hat{H}(t) = \int_0^t \hat{h}(t')dt'. \tag{6}$$

For a Poisson process, the hazard rate $\hat{h}(t)$ is a constant, independent of time. In our example of exiting state i, $\hat{h}(t) = k_{i \to}$, a constant at sufficiently long times. This is because, once the system enters state i which is in a region surrounded by high energy barriers, it will quickly thermalize (distribute itself according to the requirements of a restricted equilibrium) within state i and forget how it came there. Exit from state i is an infrequent event because of the time scale separation between the correlation time for thermalizing

within state i and the mean waiting time for escaping state i. Note the Markovian character imparted to the process by this time scale separation. For a Poisson process, then, the cumulative distribution function of waiting times has the form:

$$\hat{P}(t) = 1 - \exp\left(-k_{i\rightarrow}t\right) \tag{7}$$

and the probability density of waiting times is exponential:

$$\hat{\rho}(t) = k_{i\rightarrow} \exp\left(-k_{i\rightarrow}t\right). \tag{8}$$

The mean waiting time in state i is readily computed from Eq. (8) as $k_{i\rightarrow}^{-1}$.

In view of these definitions and properties of Poisson processes, the following computational procedure emerges for computing the rate constant $k_{i\rightarrow}$ from the reduced trajectory (sequence of visited states) onto which a MD run has been mapped. The MD run must be long enough to sample a large number of transitions out of state i. One goes through the reduced trajectory and measures all time intervals t_l between an entry into state i and the immediately following exit from i to any other state. One orders these residence times as $t_1 \leq t_2 \leq \ldots \leq t_n$, where n is the total number of visits to state i observed in the reduced trajectory. Clearly, based on the reduced trajectory, the quantity $\hat{P}(t_l) = l/n, 1 \leq l \leq n$, provides an estimate of the probability that the residence time in state i will not exceed t_l, i.e. an estimate of the cumulative probability distribution of waiting times at t_l. One forms an estimate of the cumulative hazard at t_l, $\hat{H}(t_l)$, as

$$\hat{H}(t_l) = \frac{1}{n} + \frac{1}{n-1} + \ldots + \frac{1}{n-l+1} \tag{9}$$

One then plots $\hat{H}(t_l)$ as a function of t_l for $l = 1, 2, \ldots n$. At short times the resulting hazard plot may display some curvature, associated with fast recrossing events of the dividing surfaces between state i and its surrounding states. At long times, however, if time scale separation holds, the hazard plot becomes linear. The slope at long times is the sought rate constant $k_{i\rightarrow}$. Individual rate constants $k_{i\rightarrow j}$ can readily be obtained from $k_{i\rightarrow}$ as

$$k_{i\rightarrow j} = k_{i\rightarrow} \frac{\text{Number of times exit from } i \text{ occurred to } j}{n} \tag{10}$$

The rationale behind Eq.(9) is that, for a Poisson process, the cumulative hazard $\hat{H}(t)$ is related to the cumulative probability distribution of residence times $\hat{P}_i(t)$ via Eqs. (5) and (6), hence $\hat{H}(t) = -\ln\left[1 - \hat{P}(t)\right]$. The reader can readily verify that the right-hand side of Eq.(9) is an estimate of $-\ln(1 - l/n) \simeq \int_0^{l/n} \frac{1}{1-x}dx$.

It is advisable to make sure that rate constants extracted from hazard plot analysis are invariant to the frequency of conducting minimizations along the MD trajectory to form the reduced trajectory; to ensure that no transitions are missed, the latter frequency, as well as the frequency of recording configurations along the MD trajectory, should be considerably higher than the rate constant of the fastest transition taking place in the system.

Figure 2 displays an example of a hazard plot for transition out of a state (basin of the potential energy) of a glassy binary Lennard-Jones mixture at low temperature.[27]
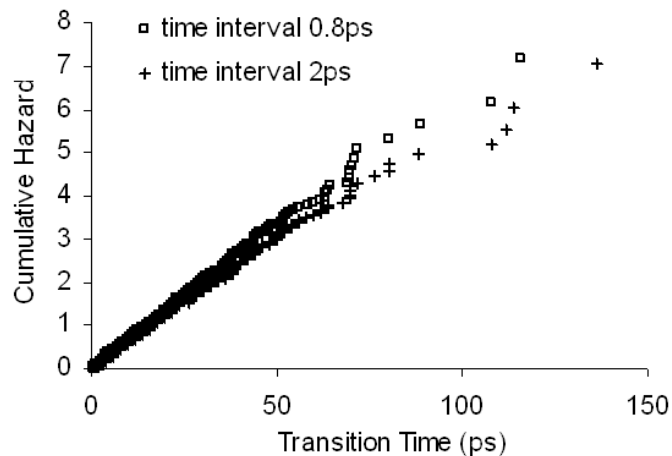
Figure 2. Hazard plot for transitions out of a given state (basin of the potential energy) for a glassy binary Lennard-Jones mixture at reduced density 1.1908 and temperature 9 K, as computed from a canonical MD simulation. Two sets of calculations are presented, one using a 0.8 ps interval between minimizations (squares) and another one using a 2 ps interval between ninimizations (crosses) in forming the reduced trajectory (sequence of states visited as a function of time).

When energy barriers between states are high in relation to $k_{\mathrm{B}}T$ and rate constants are correspondingly low, transitions between states cannot be sampled adequately by straightforward MD. One way to get around this problem is to resort to temperature-accelerated dynamics (TAD) simulations, as originally proposed by Voter and collaborators.[28] MD simulation at a higher temperature is used to access transition pathways. Waiting times obtained at the higher temperature are extrapolated down to the temperature of interest using the Arrhenius dependence of rate constants on temperature. The method has been used to great advantage in surface diffusion problems.[28] Tsalikis et al.[29] have combined microcanonical simulations at various energy levels with the histogram reweighting method to obtain rate constants in the spirit of TAD for transitions between basins in configuration space in the course of structural relaxation of a glassy binary Lennard-Jones mixture.

Infrequent event analyses based on dynamically corrected transition-state theory have found widespread use in the computation of rate constants from simulations. These analyses are based on the theory of Bennett[30] and Chandler[10], which was extended to multistate systems by Voter and Doll.[6] Let us assume that the boundary of state i in configuration space is described by an equation $C_i(\mathbf{x}) = 0$, where C_i is a continuous, differentiable function of the mass-weighted coordinates $\mathbf{x}$. $C_i(\mathbf{x}) < 0$ for all points in state i, while $C_i(\mathbf{x}) > 0$ for all points outside state i. Then, $\mathbf{n}_i = \nabla C_i(\mathbf{x})/|\nabla C_i(\mathbf{x})|$ is a unit vector normal to the boundary surface of state i at point $\mathbf{x}$ pointing towards the outside of the state. Furthermore, the function $h_i(\mathbf{x}) = 1 - H\left(C_i(\mathbf{x})\right)$, with $H(x)$ being the Heaviside step function, equals 1 if $\mathbf{x}$ belongs to state i and zero otherwise. The rate constant for transitions from i to any other state j can be expressed as

$$k_{i \to j}(t) = \frac{\langle \mathbf{n}_i\left(\mathbf{x}(0)\right) \cdot \dot{\mathbf{x}}(0) \delta\left(C_i\left(\mathbf{x}(0)\right)\right) |\nabla C_i\left(\mathbf{x}(0)\right)|\, h_j\left(\mathbf{x}(t)\right)\rangle}{P_i(\infty)} \tag{11}$$

In equation 11 the average is taken over all equilibrium dynamical trajectories of the system. The numerator has nonzero contributions from those trajectories which cross the boundary (hyper)surface of state i at time 0 and find themselves in state j after time t. The averaged quantity in the numerator is the component of the mass-weighted velocity $\dot{\mathbf{x}}$ at time 0 normal to the boundary surface of state i times a delta function along the component of $\mathbf{x}$ normal to the boundary surface which requires that the system be on that surface at time 0. The denominator is the equilibrium probability of occupancy of state i (compare equation 2). Clearly, the right-hand side of Eq.(11) has dimensions of inverse time, as expected of a rate constant. As discussed by Chandler[10] and Voter and Doll,[6] thanks to the time scale separation making exit from state i an infrequent event, $k_{i \to j}$ will practically reach a time-independent plateau value at times sufficiently longer than the time required for internal equilibration within state i.

It is useful to consider the rate constant $k_{i \to j}$ given by Eq.(11) as a product of a transition-state theory estimate of the rate constant for exiting state i times a dynamical correction factor:

$$k_{i \to j}(t) = k_{i \to}^{\text{TST}} f_{\text{d},i \to j} \tag{12}$$

Transition state theory rests on an approximation: It assumes that, whenever the system finds itself on the boundary surface of state i with momentum directed towards the outside of state i, then a successful transition out of state i will occur. In reality, this is not necessarily the case because of fast recrossings of the boundary surface at short times. Mathematically, $k_{i \to}^{\text{TST}}$ is obtained by replacing $h_j\left(\mathbf{x}(t)\right)$ in the numerator of Eq.(11) with $1 - h_i(\mathbf{x}(0^+)) = H\left(\mathbf{n}_i(\mathbf{x}(0)) \cdot \dot{\mathbf{x}}(0)\right)$. The averaging over configuration and momentum space can be separated, the momentum-space average reducing to a Boltzmann-weighted mean of the component of the mass-weighted velocity vector normal to the boundary surface over the positive semiaxis. The result is:

$$k_{i \to}^{\text{TST}} = \frac{1}{(2\beta\pi)^{1/2}} \frac{\displaystyle\int_{\text{bound. surf. of state } i} d^{f-1}x \exp\left[-\beta \mathcal{V}(\mathbf{x})\right]}{\displaystyle\int_{\text{state i}} d^f x \exp\left[-\beta \mathcal{V}(\mathbf{x})\right]} \tag{13}$$

The reader is reminded that $\mathbf{x}$ is the vector of mass-weighted coordinates of the system. The dynamical correction factor $f_{\text{d},i \to j}$, on the other hand, emerges as the ratio:

$$f_{\text{d},i \to j} = \frac{\langle \mathbf{n}_i(\mathbf{x}(0)) \cdot \dot{\mathbf{x}}(0) \delta\left[C_i(\mathbf{x}(0))\right] |\nabla C_i(\mathbf{x}(0))|\, h_j(\mathbf{x}(t))\rangle}{\langle \mathbf{n}_i(\mathbf{x}(0)) \cdot \dot{\mathbf{x}}(0) \delta\left[C_i(\mathbf{x}(0))\right] |\nabla C_i(\mathbf{x}(0))|\, [1 - h_i(\mathbf{x}(0^+))]\rangle} \tag{14}$$

which can be simplified to

$$f_{\text{d},i \to j} = \frac{\langle \mathbf{n}_i(\mathbf{x}(0)) \cdot \dot{\mathbf{x}}(0) \delta\left[C_i(\mathbf{x}(0))\right] |\nabla C_i(\mathbf{x}(0))|\, h_j(\mathbf{x}(t))\rangle}{\frac{1}{2}\langle |\mathbf{n}_i(\mathbf{x}(0)) \cdot \dot{\mathbf{x}}(0)| \delta\left[C_i(\mathbf{x}(0))\right] |\nabla C_i(\mathbf{x}(0))|\rangle} \tag{15}$$

The numerator in Eqs. (14) and (15) for $f_{d,i \to j}$ is an average over all dynamical trajectories crossing the boundary of state i which ultimately thermalize in state j. The denominator in Eq. (14) is an average over all dynamical trajectories crossing the boundary surface of state i in an outward direction. The factor $1/2$ and the absolute value of the component of velocity along the normal to the boundary surface in Eq. (15) stem from the fact that the latter component is symmetrically distributed around zero. Trajectories initiated on the boundary surface thermalize in a destination state within a correlation time that is much smaller than $(k_{i \to}^{TST})^{-1}$ and therefore their sampling entails modest computational cost. A simple sampling scheme for implementing Eq. (15) is discussed in Ref. 6.

Interestingly, in this multistate formulation for the calculation of rate constants, due to Voter and Doll,[6] transition state theory is applied to the total efflux from origin state i (see Eq. (13)). The destination state j enters only through the dynamical correction factor $f_{d,i \to j}$, computed from short dynamical trajectories initiated on the dividing surface, via Eqs. (14) or (15). For adjacent states i and j that share parts of their boundary surfaces, $f_{d,i \to j}$ starts off high (equal to the Boltzmann-weighted fraction of the boundary surface of i that is shared with j) and quickly decays with time to an asymptotic value due to dynamical recrossing and fast correlated multistate jumps. For nonadjacent states i, j the dynamical correction factor $f_{d,i \to j}$ starts off at 0 and quickly rises to an asymptotic value. This describes transitions where the system crosses the boundary surface of i, spends a short time in one or more intermediate states without thermalizing in them, then enters j, which is nonadjacent to i, and ultimately thermalizes there. Such events are referred to as fast correlated multistate jumps.

The transition-state theory expression for the rate constant for exiting state i, $k_{i \to}^{TST}$, Eq. (13), emerges as the product of half the mean absolute value of a component of the (mass-weighted) velocity along one direction in configuration space times a ratio of two configurational integrals: one taken over the boundary surface of the origin state i, and another one taken over the entire state i. Clearly, the ratio of configurational integrals has the physical meaning of a conditional probability that the system will find itself on the boundary surface, *provided* it is allowed to sample state i according to its equilibrium distribution. Instead of configurational integrals, one may consider the *partition function* Q_i of the system confined in the origin state i, as an integral over f-dimensional configuration space within state i and over f-dimensional momentum space; and the partition function $Q_i^\dagger$ of the system confined to the boundary surface of state i, as an integral over the $f - 1$ dimensions of that surface in configuration space and over the $f - 1$ dimensions of momentum space corresponding to moving within the surface, but not normal to it. Then, the expression for $k_{i \to}$ can be rewritten as

$$k_{i \to}^{TST} = \frac{k_B T}{h} \frac{Q_i^\dagger}{Q_i} \qquad (16)$$

where the factor h takes care of the different dimensionalities of the phase spaces to which the two partition functions refer. Eq. (16) is applicable beyond the classical analysis adopted here, in systems where quantum mechanical effects are important. For a system under constant pressure, where volume fluctuations are important in effecting transitions out of state i, Q_i and $Q_i^\dagger$ must be interpreted as isothermal-isobaric partition functions. Recalling the connection between Gibbs energy and isothermal-isobaric partition function,

Eq. (16) can be recast in the form

$$k_{i \to}^{\text{TST}} = \frac{k_\text{B} T}{h} \exp \left[- \left(\frac{G_i^\dagger - G_i}{k_\text{B} T} \right) \right] \tag{17}$$

An example application of Eqs. (13) and (15) to the calculation of dynamically corrected rate constants can be found in Ref. 13. There, elementary transitions of Xe and SF_6 in the pores of the zeolite Silicalite-1 were analyzed with the purpose of computing the self-diffusivity of these molecules at low occupancy. An inflexible model was invoked for the zeolite, allowing all calculations to be carried out in three dimensions ($f = 3$). States and boundary surfaces were mapped out explicitly as sets of voxels and pixels, respectively, after discretization of the intracrystalline space in the zeolite (see section 2). The configurational integrals in Eq. (13) were computed by Monte Carlo integration in these voxels and pixels.

When state i is surrounded by high potential energy ridges relative to $k_\text{B} T$ all along its boundary surface, transitions between nonadjacent states are improbable. A transition state estimate between adjacent states i and j can be obtained by analogy to Eqs. (13) and (17) as

$$k_{i \to j}^{\text{TST}} = \frac{1}{(2\beta\pi)^{1/2}} \frac{\displaystyle\int_{\text{sep. surf. between states } i \text{ and } j} d^{f-1}x \exp\left[-\beta \mathcal{V}(\mathbf{x})\right]}{\displaystyle\int_{\text{state } i} d^f x \exp\left[-\beta \mathcal{V}(\mathbf{x})\right]} \tag{18}$$

$$k_{i \to j}^{\text{TST}} = \frac{k_\text{B} T}{h} \exp \left[- \left(\frac{G_{ij}^\dagger - G_i}{k_\text{B} T} \right) \right] \tag{19}$$

In Eq. (18), the configurational integral in the numerator is taken over the part of the boundary surface of i that is common with the boundary surface of j, which we will call the separating surface between i and j. In Eq. (19), $G_{ij}^\dagger$ symbolizes the Gibbs energy of the system confined to that separating surface.

In many solid-state problems, transition between i and j is possible only through a narrow passage in the dividing surface, surrounding the first-order saddle point $(\mathbf{x}_{ij}^\dagger, \boldsymbol{\epsilon}_{ij}^\dagger)$ between the configurations $(\mathbf{x}_i, \boldsymbol{\epsilon}_i)$ and $(\mathbf{x}_j, \boldsymbol{\epsilon}_j)$ of the two local energy minima, the energy being too high ouside this narrow passage. Here $\boldsymbol{\epsilon}$ symbolizes the strain tensor with respect to a reference spatial extent of the system, usually taken as that characterizing the origin state i. Under given applied stress tensor $\boldsymbol{\sigma}$, this strain tensor may well be different between the origin state, the destination state, and the saddle point. When all the probability flux of the transition is directed through such a narrow, high-energy passage, for the purpose of computing the configurational integrals appearing in Eq. (18) one can invoke a quasiharmonic approximation, i.e. replace the potential energy with its Taylor expansion to second order with respect to $\mathbf{x}$ around a stationary point (saddle point for the numerator, minimum for the denominator) under the current volume of the system. The Gibbs energies in Eq. (19) are then estimated as

$$G_i \simeq \mathcal{V}_i + A_i^{\text{vib}} - V_i \boldsymbol{\sigma} \!:\! \boldsymbol{\epsilon}_i \tag{20}$$

$$G_{ij}^{\dagger} = \mathcal{V}_{ij}^{\dagger} + A_{ij}^{\dagger\text{vib}} - V_i \boldsymbol{\sigma}{:}\boldsymbol{\epsilon}_{ij}^{\dagger} \tag{21}$$

Here $\mathcal{V}_i$ is the potential energy at the minimum corresponding to state i and $\mathcal{V}_{ij}^{\dagger}$ is the potential energy at the saddle point corresponding to the transition state. V_i is the volume at the reference configuration used for measuring strain, usually taken as that of the origin state i, $\boldsymbol{\epsilon}_i$ is the strain tensor at the origin state and $\boldsymbol{\epsilon}_{ij}^{\dagger}$ is the strain tensor at the saddle point. A_i^{vib} is a vibrational Helmholtz energy calculated from the angular frequencies $\omega_i^{(l)}$ of the normal modes of the system at the energy minimum of the origin state, while $A_{ij}^{\dagger\text{vib}}$ is a vibrational Helmholtz energy calculated from the angular frequencies of the normal modes $\omega_{ij}^{\dagger(l)}$ at the saddle point:

$$A_i^{\text{vib}} = -k_{\text{B}}T \ln \left[\prod_{l=1}^{f} \frac{\exp(-\hbar\omega_i^{(l)}/(k_{\text{B}}T))}{1 - \exp(-\hbar\omega_i^{(l)}/(k_{\text{B}}T))} \right] \tag{22}$$

$$A_{ij}^{\dagger\text{vib}} = -k_{\text{B}}T \ln \left[\prod_{l=1}^{f-1} \frac{\exp(-\hbar\omega_{ij}^{\dagger(l)}/(k_{\text{B}}T))}{1 - \exp(-\hbar\omega_{ij}^{\dagger(l)}/(k_{\text{B}}T))} \right] \tag{23}$$

The spatial extent of the system at the minimum corresponding to the origin state is set based on the condition that G_i, as defined in Eq. (20), have a minimum with respect to the system dimensions under the applied stress $\boldsymbol{\sigma}$. Similarly, the spatial extent of the system at the saddle point is set based on the condition that $G_{ij}^{\dagger}$, as defined in Eq. (21), have a minimum with respect to the system dimensions under the applied stress $\boldsymbol{\sigma}$.[20] Kopsias[20] and Boulougouris[21] have invoked the quasiharmonic approximation approach to compute rate constants for elementary transitions in configuration space corresponding to structural relaxation of a Lennard-Jones and of an atactic polystyrene glass.

When all normal mode angular frequencies are very low relative to $k_{\text{B}}T/\hbar$ and volume changes are negligible between the origin state and the transition state, the expression for the rate constant obtained from Eqs. (19) - (23) reduces to

$$k_{i \to j}^{\text{TST}} = \frac{1}{2\pi} \frac{\prod_{l=1}^{f} \omega_i^{(l)}}{\prod_{l=1}^{f-1} \omega_{ij}^{\dagger(l)}} \exp\left[-\frac{\mathcal{V}_{ij}^{\dagger} - \mathcal{V}_i}{k_{\text{B}}T} \right] \tag{24}$$

Eq. (24) has been proposed originally by Vineyard[1] in connection with the elementary jumps executed by an isotopic atom in the course of its self-diffusion in a solid lattice.

As pointed out in section 2, in many problems it suffices to define states, transition paths, and dividing surfaces in the space of a few, slowly evolving degrees of freedom (coarse-grained variables or "order parameters"), rather than in the full $3N-3$-dimensional configuration space of the model system (assumed here to be characterized by periodic boundary conditions). In these cases, the transition-state theory estimate of the rate constant $k_{i \to j}^{\text{TST}}$ is obtainable from Eq. (18) with f being a small number, $\mathbf{x}$ being the vector of (mass-weighted) coarse-grained variables and $\mathcal{V}$ being a potential of mean force with

respect to these variables. For $f \leq 3$ it is feasible to map out this potential of mean force as a function of the coarse-grained variables. This provides a free energy profile (for $f = 1$) or landscape (for $f > 1$) that is useful for visualizing the transition.

In such lower-dimensional formulations, the configurational part of the Gibbs (or Helmholtz, in cases where volume changes are not important for the transition) energy difference $G_{ij}^{\dagger} - G_i$ appearing in Eq. (19) can be obtained through any statistical mechanics-based method designed for the computation of free energy differences. Free energy perturbation methods[31, 24, 32] offer themselves for this purpose. As the free energy barriers involved are typically large relative to $k_{\mathrm{B}}T$ (otherwise the phenomenon studied would not be an infrequent event), biased sampling techniques have to be invoked. A general strategy is umbrella sampling, wherein histograms of the relative free energy are accumulated through Boltzmann inversion of the probability density of coarse-grained variables within small overlapping windows in the space of coarse-grained variables, and different histograms are patched together to obtain the entire free energy landscape.

An example calculation of a Gibbs energy profile via umbrella sampling Monte Carlo simulation, based on work by K. Binder et al., is shown in Figure 3. The model system is an Ising model with coupling constant J between neighboring spins, consisting of $L \times L \times L$ spins arranged on a simple cubic lattice in three dimensions. Initially, the system is in a phase with all spins "down" at a temperature of $T = 0.6T_c$, lower than the critical temperature $T_c \simeq 4.51 J/k_{\mathrm{B}}$ for order- disorder transition. Then, a magnetic field $B = 0.55J$ is applied, rendering the initial phase metastable with respect to its counterpart with all spins "up". A first order phase transition ensues, which takes place via a nucleation and growth mechanism. Nuclei appear in the initial phase, each nucleus consisting of a cluster of "up" spins connected through nearest neighbor interactions. The Gibbs energy $\Delta G(n)$ for the formation of a nucleus of size (number of spins) n was accumulated by Boltzmann inversion of the size distribution of the nuclei. In addition, the Gibbs energy $\Delta G(n_{\max})$ for the largest nucleus in the system to be of size $n_{\max}$ was accumulated. The two functions are shown in Figure 3. $\Delta G(n)$ is system-size independent, while the barrier in $\Delta G(n_{\max})$ is reduced with increasing system size and would be expected to become very small for very large systems. This means that the new phase would nucleate very fast in a very large system. The barriers $\Delta G^{*}(n)$ and $\Delta G^{*}(n_{\max})$ are related via $\Delta G^{*}(n_{\max}) = \Delta G^{*}(n) - k_{\mathrm{B}}T \ln(L^3)$.[33]

A related strategy is blue moon ensemble simulation, invoked by Forester and Smith [23] in their calculations of diffusion of benzene in the zeolite silicalite-1, as mentioned in section 2 (see Figure 4).

In recent years, a variety of advanced methods have been proposed for calculating free energy profiles along a coarse-grained variable or reaction coordinate. One such method is flux-tempered metadynamics,[34] based on the metadynamics method introduced by Laio and Parrinello.[35] Metadynamics entails molecular dynamics simulation in which a repulsive Gaussian potential in a few selected coarse-grained variables is periodically added to the potential energy function of a system, to encourage its escape from the vicinity of local free energy minima with respect to these coarse-grained variables. If uniform sampling of the space of coarse-grained variables is achieved, the free energy can be estimated from the sum of added Gaussian potentials.

A general, essentially exact, but computationally intensive method for computing transition rate constants between two known states in configuration space is transition path
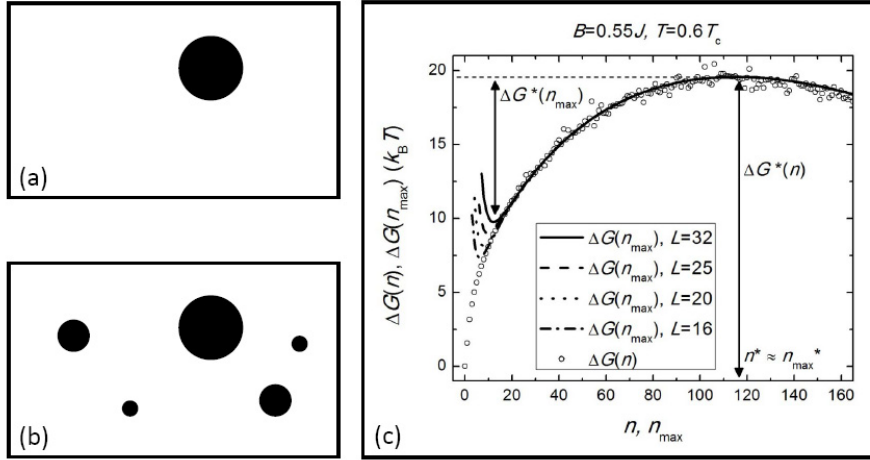
Figure 3. Gibbs energy profile for nucleation in a three-dimensional Ising model system consisting of $L \times L \times L$ sites arranged on a cubic lattice, as computed from umbrella sampling Monte Carlo simulations using spin inversions as the only moves. (a) A system containing only one nucleus. (b) A system containing multiple nuclei, the largest of which has size $n_{\max}$. (c) Gibbs energies $\Delta G(n)$ and $\Delta G(n_{\max})$ as functions of n and $n_{\max}$, respectively. The barrier heights encountered in these functions are indicated by an asterisk. See text for details.

sampling, developed by Chandler and collaborators. This method is particularly useful in complex fluid systems, where the variables participating in the reaction coordinate are difficult to anticipate. The method samples dynamical trajectories connecting the two states. These trajectories are generated and manipulated using importance sampling techniques. We will not dwell on this method here, as detailed information can be found in a number of excellent reviews.[36,37]

4   Kinetic Monte Carlo Simulation

We now turn to the question of how to track the temporal evolution of a system evolving through a sequence of infrequent events, once we know the states i, the transitions between them, and the interstate rate constants $k_{i \to j}$.

A widely used strategy is to generate a large number of stochastic trajectories of the system, conforming to the master Eq. (1). Each trajectory consists of a sequence of transitions between states. The transitions take place at times which are chosen by generation of pseudorandom numbers. The method is known as Kinetic Monte Carlo (KMC) simulation. The earliest application of KMC is thought to be Beeler's 1966 simulation of radiation damage annealing, although the term "kinetic Monte Carlo" was not widely adopted before 1990.[38]

The usual implementation of KMC relies on the following properties of Poisson processes:

- If a number of Poisson processes occur in parallel in the same system with rate constants k_i, they comprise a Poisson process with rate constant $k = \sum_i k_i$.

14
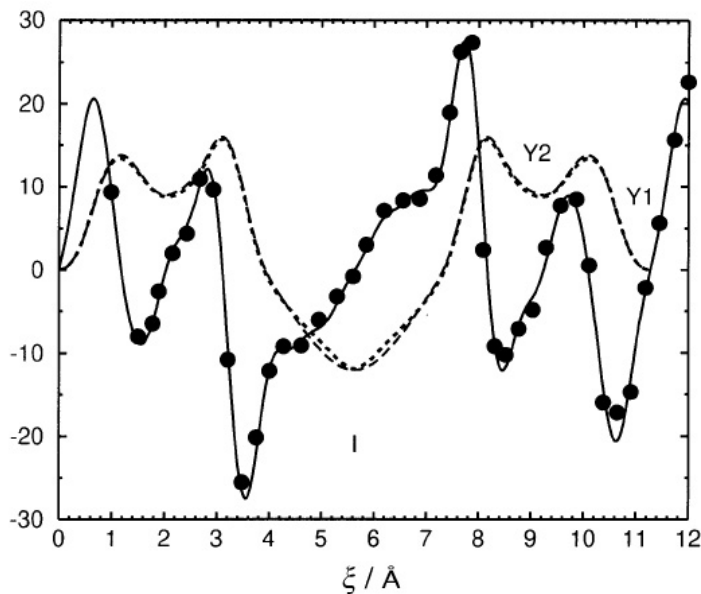
Figure 4. Configurational Helmholtz energy (potential of mean force) profile for a sorbed benzene molecule along the straight channel of the zeolite Silicalite-1, as computed by blue moon ensemble MD simulations, shown as a broken line.[23] The potential energy is measured in kJ mol^{-1}, The horizontal axis (reaction coordinate) measures the position of the center of mass of the benzene molecule projected along the axis of the channel, in Å, at room temperature. This calculation is based on a flexible model, incorporating the vibrational degrees of freedom of the zeolite. The global minimum near the center of the graph corresponds to the molecule residing within an intersection of the straight channel with a zigzag channel. Shallower minima are observed in the interior of the straight channel segments. Note that barriers in the potential of mean force are on the order of tens of kJ/mol, indicating that translational motion along the channel will proceed as a sequence of infrequent jump events. The continuous line with the points displays the derivative of the potential of mean force with respect to the reaction coordinate. This is the force needed to hold the system at a specific value of the reaction coordinate, computed via the blue moon ensemble method. The Helmholtz energy profile was obtained via numerical integration of this force.

- The waiting time of a Poisson process with rate constant k is exponentially distributed, with mean k^{-1} (see Eq.(8) and associated discussion).

- If ξ is a continuous random variable that is uniformly distributed in [0,1], then the random variable $\Delta t = -\ln(1-\xi)/k$ follows the exponential distribution with probability density $\hat{\rho}(\Delta t) = k \exp(-k\Delta t)$.

To begin the KMC simulation, a large number $\mathcal{N} >> n$ of independent walkers are deployed among the states of the system, according to a prescribed initial probability distribution among states, $P_i(0), i = 1, 2, \ldots, n$. For a system in equilibrium, $P_i(0) = P_i(\infty)$. (An easy way to generate a sample of a discrete or continuous random variable with prescribed probability distribution is to sample uniformly distributed pseudorandom values $\in [0, 1)$ for the cumulative distribution function and then find the inverse of this function at each of the sampled values. The prescription given above for sampling an exponentially distributed variable relies on the same principle.) We will use the symbol $\mathcal{N}_i(t)$ to denote

the number of walkers that find themselves in state i at time t. Initially, $\mathcal{N}_i(0)/\mathcal{N} \simeq P_i(0)$. After initialization ($t = 0$), the KMC simulation proceeds according to the following steps:

(i) For each state i that is occupied at the current time t, calculate the expected fluxes $R_{i \to j}(t) = \mathcal{N}_i(t)k_{i \to j}$ to all states j to which state i is connected. Also, compute the overall flux $R(t) = \sum_i \sum_j R_{i \to j}(t)$ and the probabilities $q_{i \to j}(t) = R_{i \to j}(t)/R(t)$.

(ii) Generate a uniformly distributed pseudorandom number[39] $\xi \in [0, 1)$. Choose the time for occurrence of the next transition in the network of states as $\Delta t = -\ln(1 - \xi)/R(t)$. Choose the type of the next transition by picking one of the possible transitions $i \to j$ according to the probabilities $q_{i \to j}(t)$.

(iii) Of the $\mathcal{N}_i(t)$ walkers present in state i, pick one with probability $1/\mathcal{N}_i(t)$ and move it to state j.

(iv) Advance the simulation time by Δt. Update the array, keeping track of the current positions of all walkers to reflect the implemented transition. Update the occupancy numbers $\mathcal{N}_i(t + \Delta t) = \mathcal{N}_i(t) - 1$ and $\mathcal{N}_j(t + \Delta t) = \mathcal{N}_j(t) + 1$.

(v) Return to step (i) to implement the next transition.

The outcome from performing this stochastic simulation over a large number of steps is a set of trajectories for all $\mathcal{N}$ walkers. Each trajectory consists of a long sequence of transitions between states of the network. Time-dependent system properties are estimated as ensemble averages over all trajectories at specific times. For example, if states correspond to sites in a three-dimensional network where a molecule can reside, one can calculate the mean square displacement along each one of the three coordinate directions as a function of time by averaging over the trajectories, and hence obtain the self-diffusivity tensor via the Einstein relation.[13,14]

When all rate constants $k_{i \to j}$ are small, KMC will take large strides Δt on the time axis. Thus, times on the order of milliseconds, seconds, or even hours can be accessed, which are prohibitive for "brute force" MD.

5 Analytical Solution of the Master Equation

When the rate constants $k_{i \to j}$ are very broadly distributed, KMC simulation may become inefficient. This is because time steps Δt must be short enough to track the fastest processes occurring in the system. With such a short Δt, processes whose rate constants are several orders of magnitude lower than those of the fastest processes can hardly be sampled. Thus, one is faced with the same long-time problem as in MD.

In such cases of great dynamical heterogeneity, it may be better to resort to a direct solution of the master equation, Eq. (1), for the time-dependent state probabilities $\{P_i(t)\}$, under prescribed initial conditions $\{P_i(0)\}$. Remarkably, this solution can be developed analytically, as discussed in Wei and Prater's classic work on the kinetics of a network of reversible chemical reactions,[8] and as detailed in recent work by Buchete and Hummer[40] and by Boulougouris.[41] We briefly outline this mathematical development here.

We start from the master equation in its matrix form, as written in Eq. (1). We transform the state probability vector $\mathbf{P}(t)$ into a reduced state probability vector $\tilde{\mathbf{P}}(t)$ with elements

$$\tilde{P}_i(t) = P_i(t)/\sqrt{P_i(\infty)} \tag{25}$$

$\tilde{\mathbf{P}}(t)$ satisfies the reduced master equation

$$\frac{\partial \tilde{\mathbf{P}}(t)}{\partial t} = \tilde{\mathbf{K}}\tilde{\mathbf{P}}(t) \tag{26}$$

with $\tilde{K}_{ij} = K_{ij}\sqrt{P_j(\infty)}/\sqrt{P_i(\infty)}$. The matrix $\tilde{\mathbf{K}}$ is symmetric by virtue of the microscopic reversibility condition, Eq. (2). One can readily show that $\tilde{\mathbf{K}}$ has the same eigenvalues as $\mathbf{K}$. These eigenvalues are real, since $\tilde{\mathbf{K}}$ is symmetric. Of these eigenvalues, one (corresponding to the establishment of the equilibrium distribution among states) is zero, and the remaining are negative. This is because $\tilde{\mathbf{K}}$ is a negative semidefinite matrix. The latter statement can be proved as follows: Let $\mathbf{y}$ be an arbitrary $n-$ dimensional vector of real elements. Then,

$$
\begin{aligned}
\mathbf{y}^{\mathrm{T}} \cdot \tilde{\mathbf{K}} \cdot \mathbf{y} = \quad & \sum_{i=1}^{n}\sum_{j=1}^{n} \tilde{K}_{ij} y_i y_j = \sum_{i=1}^{n} \tilde{K}_{ii} y_i^2 + \sum_{i=1}^{n}\sum_{\substack{j=1 \\ j\neq i}}^{n} \tilde{K}_{ij} y_i y_j = \\[2mm]
& \sum_{i=1}^{n}\left(-\sum_{\substack{j=1 \\ j\neq i}}^{n} k_{i\to j}\right) y_i^2 + \sum_{i=1}^{n}\sum_{\substack{j=1 \\ j\neq i}}^{n} k_{j\to i}\left(\frac{P_j^{\mathrm{eq}}}{P_i^{\mathrm{eq}}}\right)^{1/2} y_i y_j = \\[2mm]
& -\sum_{i=1}^{n}\sum_{\substack{j=1 \\ j\neq i}}^{n} k_{i\to j} y_i^2 + \sum_{i=1}^{n}\sum_{\substack{j=1 \\ j\neq i}}^{n} k_{i\to j}\left(\frac{P_i^{\mathrm{eq}}}{P_j^{\mathrm{eq}}}\right)^{1/2} y_i y_j = \\[2mm]
& -\tfrac{1}{2}\sum_{i=1}^{n}\sum_{\substack{j=1 \\ j\neq i}}^{n} k_{i\to j} P_i^{\mathrm{eq}}\left[\frac{y_i}{(P_j^{\mathrm{eq}})^{1/2}} - \frac{y_j}{(P_i^{\mathrm{eq}})^{1/2}}\right]^2 \leq 0 \tag{27}
\end{aligned}
$$

Eq. (27) establishes $\tilde{\mathbf{K}}$ as a negative semidefinite matrix. The proof seems to have been given for the first time by Shuler.[42] Now, if λ is one of the real eigenvalues of $\tilde{\mathbf{K}}$ with corresponding real eigenvector $\tilde{\mathbf{u}}$, then $\tilde{\mathbf{K}} \cdot \tilde{\mathbf{u}} = \lambda\tilde{\mathbf{u}}$ and therefore $\tilde{\mathbf{u}}^{\mathrm{T}} \cdot \tilde{\mathbf{K}} \cdot \tilde{\mathbf{u}} = \lambda|\tilde{\mathbf{u}}|^2$. Because $\tilde{\mathbf{K}}$ is negative semidefinite, the left-hand side of the latter equation is negative or zero, hence $\lambda \leq 0$.

Let us denote the eigenvalues of $\tilde{\mathbf{K}}$ by $\lambda_0 = 0 \geq \lambda_1 \geq \ldots \geq \lambda_{n-1}$. We symbolize by $\tilde{\mathbf{u}}_m = (\tilde{u}_{1,m}, \tilde{u}_{2,m}, \ldots, \tilde{u}_{i,m}, \ldots \tilde{u}_{n,m})$ the eigenvector of $\tilde{\mathbf{K}}$ corresponding to eigenvalue $\lambda_m, 0 \leq m \leq n-1$. The eigenvector $\tilde{\mathbf{u}}_0$ has elements $\tilde{u}_{i,0} = \tilde{P}_i(\infty) = \sqrt{P_i(\infty)}$, corresponding to the equilibrium distribution among states. The Euclidean norm of $\tilde{\mathbf{u}}_0$ is unity by the normalization of $P_i(\infty)$.

The solution to the reduced master equation can be written as:

$$\tilde{\mathbf{P}}(t) = \sum_{m=0}^{n-1}\left[\tilde{\mathbf{u}}_m \cdot \tilde{\mathbf{P}}(0)\right]\exp(\lambda_m t)\tilde{\mathbf{u}}_m = \tilde{\mathbf{P}}(\infty) + \sum_{m=1}^{n-1}\left[\tilde{\mathbf{u}}_m \cdot \tilde{\mathbf{P}}(0)\right]\exp(\lambda_m t)\tilde{\mathbf{u}}_m \tag{28}$$

where the normalization condition $\sum_{j=1}^{n} P_j(0) = 1$ has been used in separating out the

equilibrium contribution ($\lambda_0 = 0$). The eigenvectors $\tilde{\mathbf{u}}_m$ form an orthonormal basis set:

$$\tilde{\mathbf{u}}_m \cdot \tilde{\mathbf{u}}_l = \delta_{ml}, \quad 0 \le m, l \le n-1 \tag{29}$$

They also satisfy $\sum_{m=0}^{n-1} \tilde{u}_{i,m} \tilde{u}_{j,m} = \delta_{ij}$. Once $\tilde{\mathbf{P}}(t)$ has been determined, the state probabilities $\mathbf{P}(t)$ can be calculated via $P_i(t) = \tilde{P}_i(t)\sqrt{P_i(\infty)}$.

Eq. (28) has an interesting geometric interpretation, which is discussed at length by Boulougouris in the context of a general formulation for analytical solution of the master equation and calculation of time-dependent averages and autocorrelation functions which was dubbed "EROPHILE," for "Eigenvalue Representation of Observables and Probabilities in a HIgh-Dimensional Euclidean space."[41] In the n-dimensional Euclidean space spanned by the reduced state probabilities $\tilde{P}_i$, the point $\tilde{\mathbf{P}}(t)$ moves in a hyperplane that is normal to the eigenvector $\tilde{\mathbf{u}}_0 = \left(\sqrt{P_1(\infty)}, \sqrt{P_2(\infty)}, \ldots, \sqrt{P_n(\infty)} \right)$ and contains point $\tilde{\mathbf{P}}(0)$. This plane is, of course, spanned by the remaining eigenvectors $\tilde{\mathbf{u}}_1, \tilde{\mathbf{u}}_2, \ldots, \tilde{\mathbf{u}}_{n-1}$. It intersects each of the $\tilde{P}_i$ axes at $1/\sqrt{P_i(\infty)}$. As time goes by, $\tilde{\mathbf{P}}(t)$ traces a curved trajectory on this hyperplane from $\tilde{\mathbf{P}}(0)$ to the equilibrium distribution $\tilde{\mathbf{P}}(\infty)$.

Let us consider any observable, $\mathcal{A}$, which has well-defined values $\mathcal{A}_i$ within each of the states i. The (nonequilibrium) ensemble average $\langle \mathcal{A}(t) \rangle$ at any time t is

$$\langle \mathcal{A}(t) \rangle = \sum_{i=1}^{n} P_i(t) \mathcal{A}_i = \langle \mathcal{A}(\infty) \rangle + \sum_{m=1}^{n-1} a_m \beta_m \exp\left(\lambda_m t\right) \tag{30}$$

where

$$a_m = \tilde{\mathbf{u}}_m \cdot \tilde{\mathbf{P}}(0) \tag{31}$$

and

$$\beta_m = \tilde{\mathbf{u}}_m \cdot \tilde{\boldsymbol{\mathcal{A}}} \tag{32}$$

In Eq. (32), $\tilde{\boldsymbol{\mathcal{A}}}$ is an n-dimensional vector with elements $\tilde{\mathcal{A}}_i = \mathcal{A}_i \sqrt{P_i(\infty)}$, formed from the values $\mathcal{A}_i$ of the observable in each state and the equilibrium probabilities $P_i(\infty)$ of the states.

Eq. (30) expresses the time-dependent ensemble average of the observable, $\langle \mathcal{A}(t) \rangle$, as a sum of its value $\langle \mathcal{A}(\infty) \rangle$ when equilibrium among all n states has been established, plus a sum of exponentially decaying functions. The sum is taken over all relaxation modes, with characteristic time constants $-1/\lambda_1 \ge -1/\lambda_2 \ge \ldots \ge -1/\lambda_{n-1}$.

In the space spanned by $\tilde{P}_i$, considered above, one can draw the vector $\tilde{\boldsymbol{\mathcal{A}}}$ with components $\tilde{\mathcal{A}}_i = \mathcal{A}_i \sqrt{P_i(\infty)}$ along each $\tilde{P}_i$ axis. The equilibrium average $\langle \mathcal{A}(\infty) \rangle$ is interpreted geometrically as the projection of this vector on the eigenvector $\tilde{\mathbf{u}}_0 = \tilde{\mathbf{P}}(\infty)$. The time-dependent average $\langle \mathcal{A}(t) \rangle$, on the other hand, is interpreted as a projection of the same vector on the reduced probability vector $\tilde{\mathbf{P}}(t)$. As the tip of $\tilde{\mathbf{P}}(t)$ moves from $\tilde{\mathbf{P}}(0)$ toward the equilibrium point $\tilde{\mathbf{P}}(\infty)$, $\langle \mathcal{A}(t) \rangle$ moves to $\langle \mathcal{A}(\infty) \rangle$. The exponentially decaying components of $\langle \mathcal{A} \rangle$ along the modes are proportional to the projections β_m of $\tilde{\boldsymbol{\mathcal{A}}}$ on the eigenvectors.[41]

One can readily express time autocorrelation functions for observables using the analytical solution to the reduced master equation. For any observable $\mathcal{A}$ defined in the states,

$$\langle \mathcal{A}(0)\mathcal{A}(t)\rangle - \langle \mathcal{A}(0)\rangle \langle \mathcal{A}(\infty)\rangle = \sum_{m=1}^{n-1} \beta_m^2 \exp\left(\lambda_m t\right) + \langle \mathcal{A}(\infty)\rangle \sum_{m=1}^{n-1} a_m \beta_m \exp\left(\lambda_m t\right) +$$
$$\sum_{m=1}^{n-1} \beta_m \exp\left(\lambda_m t\right) \sum_{l=1}^{n-1} \beta_l \sum_{k=1}^{n-1} \sum_{i=1}^{n} \left[\frac{a_k \tilde{u}_{i,l}\tilde{u}_{i,m}\tilde{u}_{i,k}}{\tilde{P}_i(\infty)}\right] \qquad (33)$$

In the special case where the system is initially distributed among states according to equilibrium, $\tilde{\mathbf{P}}(0) = \tilde{\mathbf{P}}(\infty)$, by virtue of the orthonormality of eigenvectors we have $a_m = 0, m = 1, 2, \ldots, n-1$ and Eq. (33) simplifies to

$$\langle \mathcal{A}(0)\mathcal{A}(t)\rangle - \langle \mathcal{A}(\infty)\rangle^2 = \sum_{m=1}^{n-1} \beta_m^2 \exp\left(\lambda_m t\right) \qquad (34)$$

In this special case, $\left\langle (\delta\mathcal{A})^2 \right\rangle^{1/2} = \left[\langle \mathcal{A}(0)\mathcal{A}(t)\rangle - \langle \mathcal{A}(\infty)\rangle^2\right]^{1/2}$ can be interpreted geometrically as the length of the projection of vector $\tilde{\boldsymbol{\mathcal{A}}}$ on the on the $n-1$-dimensional hyperplane on which $\tilde{\mathbf{P}}(t)$ moves.[41]

Implementation of this analytical solution scheme requires that the equilibrium state probabilities $P_i(\infty)$ be found at the beginning of the calculation. An easy strategy for accomplishing this without diagonalizing matrix $\mathbf{K}$ is to use the iterative successive substitution scheme:[43]

$$P_i^{(l+1)}(t) = \frac{\sum_{j\neq i} P_j^{(l)}(t)k_{j\to i}}{\sum_{j\neq i} k_{i\to j}} \qquad (35)$$

Implementation of Eq. (28) requires diagonalization of the singular symmetric $n \times n$ matrix $\tilde{\mathbf{K}}$.

For spatially periodic systems, in which the set of states is obtainable by replication of a "unit cell" of states in one, two, or three dimensions, Kolokathis[44] has developed a method for calculating the eigenvalues and eigenvectors of the reduced rate constant matrix of the whole system by diagonalizing matrices of dimension corresponding to a single unit cell. This Master Equation Solution by Recursive Reduction of Dimensionality (MESoRReD) in diagonalizing the rate constant matrix method greatly reduces the computational effort required for diagonalization and is valuable in addressing problems of diffusion in crystalline solids.

6 Example: Diffusion of Xenon in Silicalite

Zeolites are crystalline aluminosilicates whose crystal structure is characterized by the presence of regular cavities and pores of diameter commensurate with the sizes of common gas or solvent molecules. This structure imparts to zeolites a unique ability to distinguish among molecules sorbed in their pores in terms of their size, shape, and charge distribution and forms the basis for a large number of technological applications of zeolites as industrial separation media, catalysts, and ion exchange agents.

Diffusivities in zeolites are commonly computed via MD simulations. In many systems of practical relevance, however, diffusion is too slow to be computed reliably by MD. For example, as can be seen in Figure 4, benzene experiences a tight fit in the pores of silicalite-1, such that moving from an intersection region to the interior of a straight channel requires overcoming a free energy barrier of approximately 27 kJ/mol. A MD simulation of benzene sorbed at low occupancy in silicalite at room temperature would exhaust itself tracking local motions of the benzene within a sorption site and would hardly sample any jumps into other sorption sites, which contribute to translational diffusion. A reasonable prediction of the diffusivity can only be obtained through computation of rate constants for jumping from site to site via infrequent event analysis and solution of the master equation in the network of sorption sites (states). [14, 23]

A simple sorbate/zeolite system on which infrequent event-based calculations appear to have been conducted for the first time is xenon (Xe) in silicalite-1 at low temperatures and occupancies. Here we review briefly some calculations on this system at 150 K, coming from the early work of June et al. [13] and the very recent work of Kolokathis. [44] The unit cell of silicalite has the chemical constitution $Si_{96}O_{192}$. Calculations were conducted with its orthorhombic form, which has lattice parameters $a = 20.07$ Å, $b = 19.92$ Å, $c = 13.42$ Å along the x, y, and z directions, respectively. The zeolite possesses two intersecting systems of channels, both of diameter around 5.5 Å: Straight channels, which run along the b crystallographic axis, and sinusoidal, or zig-zag, channels, which run along the a crystallographic axis. The channel systems come together at intersections, which are more spatious (diameter around 9 Å).

In the modeling work of June et al., [45, 13] silicalite was considered as rigid and its interaction with Xe was described as a sum of Lennard-Jones potentials between each oxygen in its framework and the Xe molecule. An efficient potential pretabulation and interpolation scheme in three dimensions was developed for this potential in simulations. [45] June et al. [13] conducted a thorough analysis of the potential energy hypersurface experienced by Xe in silicalite as a function of its three translational degrees of freedom, identified states and transitions between them, and computed rate constants $k_{i \to j}$ using Transition State Theory (TST) with or without dynamical corrections. This analysis led to the identification of 12 states per unit cell for Xe in silicalite at very low loadings. There are four states per unit cell in the interior of straight channel segments (S), four states per unit cell in the interior of zig-zag channel segments (Z) and four states per unit cell in intersections (I). Of these, Z and S states are more favorable, while I, where the dispersive attraction of Xe with the surrounding zeolite lattice is weaker, is less favorable. At 150 K the equilibrium probabilities of occupancy of these states, normalized within one fourth of the unit cell, are $P_Z^{eq} = 0.572$, $P_S^{eq} = 0.414$, $P_I^{eq} = 0.014$. The spatial arrangement of these states within one unit cell of silicalite is shown in Figure 5.

There is a rich connectivity among the states for Xe in silicalite. Apart from I to S and I to Z transitions, June et al. [13] identified direct transitions between S and Z states which circumvent the intersection regions. There are eleven distinct types of transitions. These types and their associated rate constants, as calculated by Transition State Theory without dynamical corrections [Eq. (18)], are shown in Table 1.

Figure 6 provides a pictorial depiction of the spatial arrangement of sorption states 1-12 in a central unit cell (outlined with green borders) and of the periodic images of these states located to the right (R) and left (L) of the central unit cell. States 1-4 are I states;
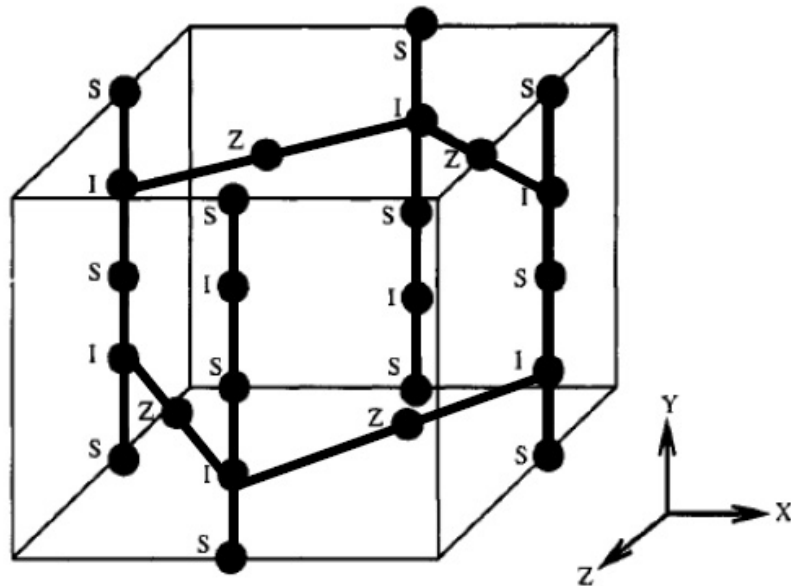
Figure 5. Schematic outline of the pore structure of a unit cell of silicalite. Spheres represent the three types of sorption states (Z = sinusoidal channel state, S = straight channel state, and I = intersection state) on the zeolite-sorbate potential hypersurface. The thick lines provide a rough depiction of the axes of straight and sinusoidal (zig-zag) channels.

states 5-8 are S states; and states 9-12 are Z states. Figure 6 also shows the network of transitions as a set of straight line segments connecting the states. Each I, S, and Z state is connected to another 4, 6, and 8 states, respectively. Thus, there are 72 transition pathways going in and out of a unit cell. These transitions are summarized in the third column of Table 1; to each of these transitions a rate and a type are assigned in the first two columns of the same table.

Table 2 shows estimates of the diffusivities D_{xx}, D_{yy}, D_{zz}, as well as of the orientationally averaged diffusivity $D = (D_{xx} + D_{yy} + D_{zz})/3$ at 150 K, obtained from the states, connectivity, and rate constant information of Figures 5, 6 and Table 1. No distinction is made between self- and transport diffusivities, as the two are equal at the very low occupancies considered here. Diffusivities have been calculated by three methods:

- Kinetic Monte Carlo simulation: Here one deploys a large number (e.g. 4000) of noninteracting Xe molecules ("walkers") among the states of a large (e.g. $10 \times 10 \times 10$ unit cells) network with periodic boundary conditions, according to the equilibrium occupancy probabilities of the states. One then generates a long (e.g., at least 27000 steps, corresponding to roughly 18 ns for the Xe/silicalite-1 system) KMC trajectory by the procedure discussed in Section 4. The diffusivity is calculated via the Einstein

Type of Transition	Rate constant $k_{i \to j}$ (s^{-1})	Transitions
I $\to$ S	1.309×10^{11}	$1 \to 5, 1 \to 6, 2 \to 5, 2 \to 6,$ $3 \to 7, 3 \to 8, 4 \to 7, 4 \to 8$
S $\to$ I	4.444×10^{9}	$5 \to 1, 5 \to 2, 6 \to 1, 6 \to 2,$ $7 \to 3, 7 \to 4, 8 \to 3, 8 \to 4$
I $\underset{a}{\to}$ Z	2.958×10^{10}	$1 \to 9, 2 \to 12, 3 \underset{L}{\to} 10, 4 \to 11$
Z $\underset{a}{\to}$ I	7.241×10^{8}	$9 \to 1, 10 \underset{R}{\to} 3, 11 \to 4, 12 \to 2$
I $\underset{b}{\to}$ Z	1.501×10^{10}	$1 \to 10, 2 \to 11, 3 \to 9, 4 \underset{L}{\to} 12$
Z $\underset{b}{\to}$ I	3.673×10^{8}	$9 \to 3, 10 \to 1, 11 \to 2, 12 \underset{R}{\to} 4$
S $\underset{a}{\to}$ Z	3.974×10^{8}	$5 \to 9, 6 \to 9, 7 \underset{L}{\to} 10, 8 \underset{L}{\to} 10,$ $7 \to 11, 8 \to 11, 5 \to 12, 6 \to 12$
Z $\underset{a}{\to}$ S	2.853×10^{8}	$9 \to 5, 9 \to 6, 10 \underset{R}{\to} 7, 10 \underset{R}{\to} 8,$ $11 \to 7, 11 \to 8, 12 \to 5, 12 \to 6$
S $\underset{b}{\to}$ Z	8.567×10^{8}	$5 \to 10, 5 \to 11, 6 \to 10, 6 \to 11,$ $7 \to 9, 7 \underset{L}{\to} 12, 8 \to 9, 8 \underset{L}{\to} 12$
Z $\underset{b}{\to}$ S	6.150×10^{8}	$10 \to 5, 11 \to 5, 10 \to 6, 11 \to 6,$ $9 \to 7, 12 \underset{R}{\to} 7, 9 \to 8, 12 \underset{R}{\to} 8$
Z $\to$ Z	9.737×10^{8}	$9 \to 10, 9 \underset{L}{\to} 10, 10 \to 9, 10 \underset{R}{\to} 9,$ $11 \to 12, 11 \underset{L}{\to} 12, 12 \to 11, 12 \underset{R}{\to} 11$

Table 1. Rate constants[13] for interstate transitions of xenon in silicalite at 150 K as calculated from Transition-State Theory in tree dimensions, without dynamical corrections. I, S, and Z represent an intersection, straight channel state and sinusoidal channel state, respectively. The indices under the arrows distinguish between different transitions starting at the same origin state and ending at different images of the destination state
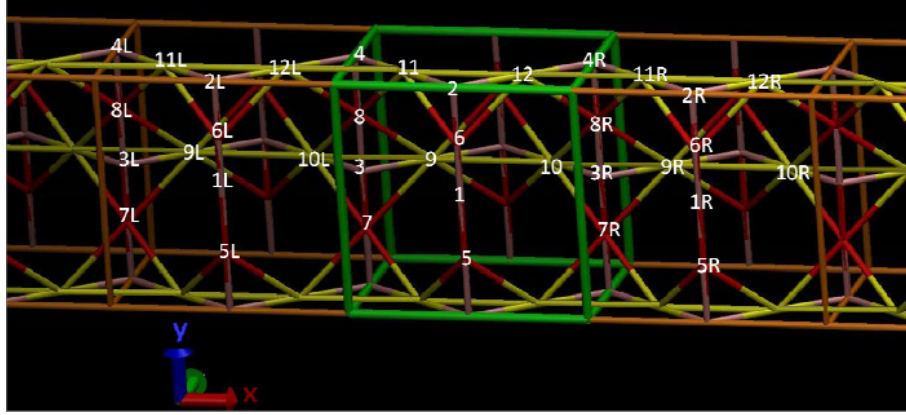
Figure 6. Transitions of Xe in silicalite-1, depicted as straight lines in three-dimensional space. Red color shows S (straight-channel) states, yellow color shows Z (zig-zag channel) states and pink color shows I (intersection) states. Green box defines the borders of one unit cell. Orange color shows the borders of cells along the x axis.

relation, e.g.

$$D_{xx} = \lim_{t \to \infty} \frac{\left\langle [x(t) - x(0)]^2 \right\rangle}{2t} \tag{36}$$

and similarly for y and z. Table 2 presents KMC results from both the original work of June et al.[13] and the very recent calculations of Kolokathis.[44] The two sets of KMC are indistinguishable, within simulation error.

- Numerical solution of the master equation. Here, the master equation, Eq. (1), was solved numerically as an initial value problem with the Euler method to determine the state occupancy probabilities as functions of time. The calculation was performed on a system of $50 \times 50 \times 50$ unit cells with periodic boundary conditions. Initially, a probability of 1 was assigned to an S state at the center of the system, all other states being empty. The integration time step in the Euler method was 10^{-12} s. State probabilities from the numerical solution were summed at the level of unit cells and divided by the unit cell volume to obtain the probability density $\rho_{\text{cell}}(x, y, z, t)$. The marginal probability densities along the three directions, $\rho_{\text{cell},x}(x,t)$, $\rho_{\text{cell},y}(y,t)$, $\rho_{\text{cell},z}(z,t)$ were then calculated. The diffusivities D_{xx}, D_{yy}, D_{zz} were obtained by matching these time-dependent probability densities to the solution of the corresponding continuum diffusion problem. For the maximum time used in the Euler integration, 10 ns, this is indistinguishable from the Gaussian

$$\rho_{\text{cell},x}(x,t) = \frac{1}{\sqrt{4\pi D_{xx}t}} \exp\left[-\frac{(x-x_0)^2}{4D_{xx}t} \right] \tag{37}$$

and similarly for y and z.

- Analytical solution of the master equation. Model systems consisting of $2^7 = 128$ adjacent unit cells arranged in a linear array along the x, y, or z directions, with

periodic boundary conditions at the ends, were considered. The symmetrized rate constant matrix $\tilde{\mathbf{K}}_{27}$ for each of these systems was formed and diagonalized. Initially, all probability was distributed in the central two unit cells of the array. The time-dependent probability of occupancy of all states in the system was calculated as a sum of exponentially decaying functions of time using the eigenvectors and eigenvalues of matrix $\tilde{\mathbf{K}}_{27}$, according to Eqs. (25) and (28). To avoid the time-consuming diagonalization of the 1536×1536-dimensional matrix $\tilde{\mathbf{K}}_{27}$, a recursive reduction scheme was devised,[44] which ultimately expresses the eigenvalues and eigenvectors of $\tilde{\mathbf{K}}_{27}$ in terms of the eigenvalues and eigenvectors of the symmetrized rate constant matrix for a single unit cell, $\tilde{\mathbf{K}}_1$ and other 12×12 matrices that can be formed readily from the set of rate constants. This MESoRReD scheme[44] affords great savings in CPU time. The calculation of diffusivities from the time-dependent state probability profiles is again accomplished by fitting the solution to the corresponding continuum diffusion equation to the master equation results.

Method	D_{xx} (m^{2}s^{-1})	D_{yy} (m^{2}s^{-1})	D_{zz} (m^{2}s^{-1})	D (m^{2}s^{-1})
June et al. MD[13]	4.3×10^{-10}	1.0×10^{-9}	0.99×10^{-10}	5.1×10^{-10}
June et al. KMC-DC TST[13]	5.1×10^{-10}	7.3×10^{-10}	0.83×10^{-10}	4.41×10^{-10}
June et al. KMC-TST[13]	1×10^{-9}	1.2×10^{-9}	1.7×10^{-10}	7.9×10^{-10}
KMC-TST[44]	9.75×10^{-10}	1.21×10^{-9}	1.71×10^{-10}	7.85×10^{-10}
Euler Method TST[44]	9.70×10^{-10}	1.25×10^{-9}	1.83×10^{-10}	8.01×10^{-10}
Master Eq. Soln. by Recursive Reduction of Dimensionality[44]	9.71×10^{-10}	1.17×10^{-9}	1.75×10^{-10}	7.71×10^{-10}
PFG-NMR[53,54]	-	-	-	1.633×10^{-10}

Table 2. Diffusion coefficients for xenon in silicalite-1 at 150 K as computed by different methods and as measured experimentally

As seen in Table 2, estimates of D_{xx}, D_{yy}, D_{zz} and D obtained by different TST-based methods are within 3% of each other. Estimates based on rate constants computed via *dy-*

Method	CPU time (s)	Memory (MB)
June et al. MD[13]	309173.00	
Euler method[44]	23760.00	401
KMC[44]	6183.46	6
Master Eq. Soln. by Recursive Reduction of dimensionality[44]	2.96	42

Table 3. CPU time and memory (RAM) requirements for calculating the diffusivity of Xe in silicalite-1 at 150 K with a relative error of 3% by various methods. All times except that for MD were measured[44] on an Intel Celeron CPU E200 system with 1.99 GB RAM, running at 2.40 GHz. The time for MD is an estimate, based on the work of June et al.[13] The CPU time required for the method of analytical solution of the master equation by recursive reduction of dimensionality of the rate constant matrix is partitioned as follows: (a) Determination of the time-dependent state probabilities 0.27 s; (b) Determination of diffusivity by fitting the profile of state probabilities with the solution to the continuum diffusion equation 2.69 s.

namically corrected TST, i.e., using Eqs. (12), (13) and (15), obtained by June et al. [13] are also included in the Table, for comparison. Consideration of dynamical corrections gives lower rate constants for interstate transitions (mainly due to recrossings of the dividing surfaces) and therefore lower diffusivities. Estimates from the dynamically corrected TST are very close to those obtained by direct MD simulation, which can be considered as the "exact results" for the force field employed. In table 2 is also shown the single experimental value of the orientationally averaged self-diffusivity D available for Xe in silicalite-1 at 150 K via pulsed field gradient nuclear magnetic resonance (PFG-NMR) experiments using ^{129}Xe. The experimental value is of the same order as, but considerably lower than, the best simulation estimates from MD and DC-TST. This is partly due to the fact that the intracrystalline occupancy was finite in the experiments, rather than tending to zero, as considered in the simulations. Imperfections in the zeolite crystals employed in the experiment and in the force field employed in the simulations and the fact that the high-temperature, orthorhombic form of the crystal was used in the simulations at 150 K no doubt contribute to the difference between experimental and predicted values.

The computational requirements of MD and of the TST-based methods for computing the diffusivity of Xe in silicalite-1 to the same level of accuracy are compared in Table 3. Clearly, analytical solution of the master equation for a periodic model system, based on recursive reduction of the rate constant matrix, is the most efficient among the methods examined; its CPU time requirement is smaller than that of MD, numerical solution of the master equation by the Euler method, and Kinetic Monte Carlo by factors of 100000, 8000, and 2100, respectively. The widely practiced KMC comes next. For penetrants

experiencing a close fit in zeolite pores, such as benzene in silicalite, MD is incapable of tracking diffusional progress and infrequent event-based methods remain as the only viable alternative.[14, 23]

7 Example: Diffusion of CO_2 in Poly(amide imide)

Knowing the diffusion coefficient of small (gas, solvent) molecules in glassy polymers is of great importance to the design of packaging materials with controlled barrier properties, as well as of separation membranes with tailored permeability and selectivity.[19] While the problem of diffusion in molten and rubbery polymer matrices at temperatures sufficiently above the glass temperature T_g can be addressed successfully via MD simulation, diffusion in polymer glasses is too slow to be predictable by direct MD. The self-diffusivities of gases dissolved at low concentration in glassy polymers are typically on the order of $10^{-12} \mathrm{m^2/s}$ and would require simulation times longer than μs in order to be predicted by MD from the mean square displacement $\left\langle [\mathbf{r}(t) - \mathbf{r}(0)]^2 \right\rangle$ via the Einstein relation:

$$D_s = \lim_{t \to \infty} \frac{\left\langle [\mathbf{r}(t) - \mathbf{r}(0)]^2 \right\rangle}{6t} \tag{38}$$

The presence of an "anomalous diffusion" regime at short times, where $\left\langle [\mathbf{r}(t) - \mathbf{r}(0)]^2 \right\rangle$ rises sublinearly with time (see below) makes the reliable calculation of D_s even more demanding.

MD simulations have established that the diffusion of a small molecule in a glassy polymer takes place as a sequence of infrequent jumps between accessible volume clusters within the polymer. Thus, the problem of calculating the self-diffusivity in an amorphous glassy polymer is similar to that in a zeolite, with the following important differences: (a) Simulating the structure of the amorphous polymer is a challenge in itself, which has stimulated significant methodological development. Currently, a satisfactory strategy for generating glassy polymer configurations is to coarse-grain an atomistic model into one involving fewer degrees of freedom, equilibrate the coarse-grained model at all length scales using connectivity-altering Monte Carlo algorithms, reverse-map back to the atomistic level to obtain well-equilibrated melt configurations, and finally quench to the glassy state.[55] (b) infrequent-event analyses of elementary jumps only in the penetrant degrees of freedom, assuming an inflexible polymer matrix, are of very limited utility; the motion of polymer degrees of freedom in the course of a diffusive jump must be taken into account in calculating rate constants for the elementary diffusive jumps in order to obtain a realistic estimate of D_s.

The first serious calculation of diffusivities in an amorphous polymer matrix based on TST concepts was performed by Gusev and Suter.[56] This calculation is based on the idea that atoms of the polymer matrix execute harmonic vibrations around their equilibrium positions in the minimum energy configuration of the penetrant-free polymer. For a spherical penetrant, this leads to a three-dimensional free energy field that can be expressed in terms of additive contributions depending on the distances of the center of the penetrant from the equilibrium positions of the polymer atoms. All (three-dimensional) states and (two-dimensional) dividing surfaces for translational motion of the penetrant in the polymer matrix are determined via steepest descent constructions in this free energy function,

in a similar way as in rigid zeolite models (compare Sections 2 and 6) and transition rate constants for all elementary jumps were determined via Eq. (18) with $f = 3$ and the free energy field including vibrational contributions from polymer atoms playing the role of $\mathcal{V}(\mathbf{x})$. The amplitude of polymer atom vibrations, Δ, is usually treated as an adjustable parameter. A self-consistent method has been proposed for its determination from short-time MD simulations of the polymer matrix.[57] This is a useful and computationally efficient approach if the penetrant is small enough to justify the assumption of harmonic ("elastic") motion of matrix atoms.

Greenfield[15,58,59] developed a multidimensional TST approach for diffusion in a glassy polymer, where polymer degrees of freedom are taken into account explicitly in the reaction coordinate of the infrequent events whereby diffusion takes place. For the identification of states and dividing surfaces, Greenfield introduced a method based on geometric analysis of accessible volume within penetrant-free minimum energy configurations of the glassy polymer, which has been outlined briefly in section 2. This calculation goes from geometrically identified "necks" between accessible volume clusters to saddle points in the multidimensional configuration space of the penetrant plus polymer system, to transition paths in that configuration space. Each transition path connects two basins (regions around local minima) i and j in multidimensional configuration space, with the center of mass of the penetrant residing in one cluster of accessible volume in basin i and in another cluster of accessible volume in basin j. The rate constant $k_{i \to j}$ for the jump between i and j is calculated in the harmonic approximation via Eqs. (19 - 23) with the stress set to zero and volume changes neglected. In general, there are many basins corresponding to the penetrant residing in the same cluster of accessible volume as in basin i; these basins communicate with each other via facile transitions and are envisioned as constituting a "macrostate" or "metabasin" I. Similarly, basin j belongs to a larger "metabasin" J. The rate constant for transition between metabasins I and J is estimated as

$$k_{I \to J} = \sum_{i \in I} \sum_{j \in J} k_{i \to j} \frac{P_i(\infty)}{P_I(\infty)} \tag{39}$$

The ratio $P_i(\infty)/P_I(\infty)$ is estimated from a short MD simulation of the polymer plus penetrant system with the penetrant confined in the accessible volume of metabasin I; it is the ratio of time spent in basin i to that spent in the entire metabasin I. The rate constants $k_{I \to J}$ constitute a rate constant matrix $\mathbf{K}$ providing a stochastic description of the motion of the penetrant at the level of metabasins, or clusters of accessible volume. They may have to be adjusted to ensure that microscopic reversibility, Eq. (2), is satisfied.

Vergadou[60] extended and applied Greenfield's method to study permeation of CO_2 in a glassy poly(amide imide) of complex repeat unit constitution [-NH-C$_6$H$_4$-C(CF$_3$)$_2$-C$_6$H$_4$-NH-CO-C$_6$H$_4$(CH$_3$)-N(CO)$_2$C$_6$H$_3$-CO-]$_n$. All multidimensional TST calculations were performed in atomic Cartesian coordinates. The distribution of rate constants for elementary jumps $k_{i \to j}$ was found to be very broad, covering the range 10^{-14} to 10^{-1} s^{-1}, and skewed towards low values, the most probable value being around 10^{-6} s^{-1}. The distribution of elementary jump lengths of the penetrant, on the other hand, was found to be relatively narrow, covering the range 2 to 10 Å, with a most probable value around 4 Å. Figure 7 displays three characteristic snapshots in the course of an elementary jump of a CO_2 molecule. The initial and final configurations constitute local minima of the potential energy of the polymer plus penetrant system, while the middle configuration (transition
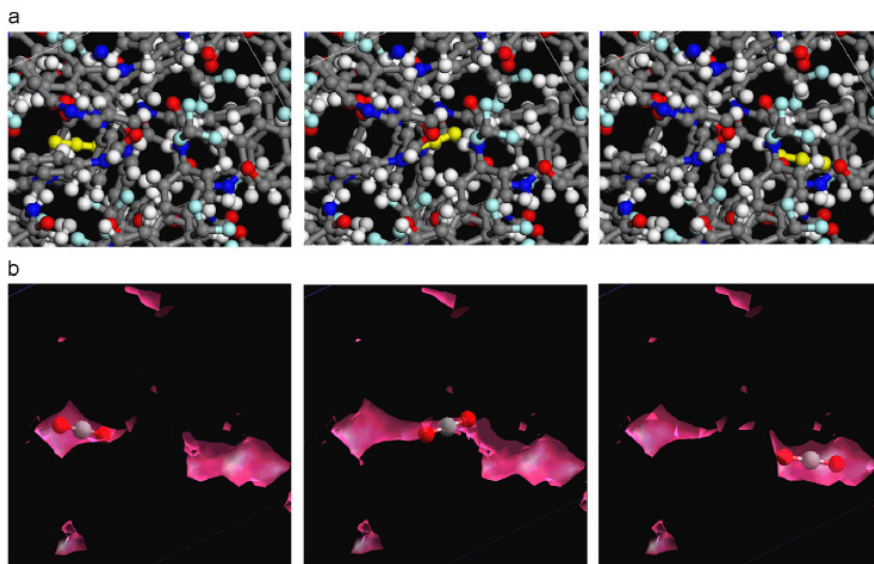
Figure 7. (a) Snapshots along the transition path of an elementary jump of a CO_2 molecule within an amorphous poly(amide imide) (PAI) matrix. The configurations on the left and right correspond to local minima of the potential energy of the CO_2 + PAI with respect to all atomic coordinates. The configuration in the middle corresponds to a saddle point of the potential energy. (b) Visualization of the accessible volume of the polymer, as determined using a spherical probe of radius $1.3\,\text{Å}$ in the same three snapshots along the transition path. The CO_2 penetrant is also shown. In the saddle point configuration, polymer degrees of freedom have moved in such a way as to form a "neck" connecting the accessible volume clusters in the initial and final states. The orientation of the CO_2 at the saddle point is more or less parallel to this neck of accessible volume.

state) is a saddle point of the potential energy function. Molecular configurations are shown in part a of the figure, while part b displays the accessible volume distribution at these three characteristic points along the transition path of the elementary jump. Clearly, in the initial and final states the CO_2 molecule lies in the interior of accessible volume clusters formed among the atoms of the glassy polymer. In the transition state a "neck" of accessible volume has developed which momentarily connects the origin and destination clusters, letting the penetrant go through. At the transition state the penetrant is oriented roughly parallel to this neck. Evidently, the degrees of freedom of the polymer and the orientational degrees of freedom of the penetrant play a significant role in shaping the transition path and hence the rate constant of the elementary jump.

After calculating all relevant rate constants $k_{I \to J}$ by multidimensional TST, the diffusive progress of CO_2 in the PAI matrix was tracked via Kinetic Monte Carlo simulation, applying periodic boundary conditions at the simulation cell boundaries (see Section 4). Figure 8 displays the mean square displacement $\left\langle [\mathbf{r}(t) - \mathbf{r}(0)]^2 \right\rangle$ from KMC trajectories as a function of elapsed time in log-log (left) and linear (right) coordinates. A strongly anomalous regime ($\left\langle [\mathbf{r}(t) - \mathbf{r}(0)]^2 \right\rangle \propto t^n$ with $n < 1$) is observed at short times. Beyond 1 μs, however, where the root mean square displacement exceeds the dimension L of the periodic simulation box, the dependence becomes linear, allowing one to extract the self-

28

diffusion coefficient as one sixth the slope of the right-hand side plot, in linear coordinates [compare Eq. (38)].

The presence of an anomalous regime at short times has by now been well established from simulations of transport in amorphous polymers. Anomalous diffusion is due to long-lived structural correlations in the polymer, which cause the diffusant to encounter a locally heterogeneous environment. From a practical point of view, anomalous diffusion increases the computational cost of simulations required for the prediction of D_s, since such simulations must be long enough for the Einstein (exponent $n = 1$) regime to be adequately sampled. In glassy polymer matrices, the crossover from anomalous to normal diffusion is often observed at root mean squared penetrant displacements roughly equal to the simulation box size. This is a system size effect. At length scales larger than the simulation box size, the model matrix looks like a regular lattice to the penetrant; structural heterogeneities leading to anomalous diffusion are suppressed, precipitating a premature onset of the Einstein regime. Based on the work of Karayiannis,[61] despite this premature onset, the estimate of D_s extracted from the linear part of the mean square displacement versus time curves is not significantly affected by system size, provided the model structures employed in the simulation are large enough and numerous enough. Karayiannis [61] has conducted a systematic KMC study and Effective Medium Theory analysis of the relation between the duration of the anomalous diffusion regime and the heterogeneity in the distribution of elementary jump rate constants.

Based on Figure 8, the duration of the anomalous regime for diffusion of CO_2 in PAI is at least 1 μs. State-of-the-art measurements of CO_2 diffusion in glassy polymers with carbon-13 Pulsed Field Gradient NMR indicate that it may take 10 ms for motion of the penetrant to become fully isotropic and the Einstein regime to be reached.[62]

From the slope of the Einstein regime of Figure 8 we extract a diffusivity value for the diffusion of CO_2 in PAI at low concentration equal to $D_s = 0.25 \times 10^{-12} \text{m}^2\text{s}^{-1}$. An experimental estimate is[63] $D_s = 0.81 \times 10^{-12} \text{m}^2\text{s}^{-1}$. The solubility coefficient of CO_2 in the PAI, estimated by the Widom test particle insertion method[31] based on the same atomistic model, is $S = 0.42 \text{ cm}^3(\text{STP})/(\text{cm}^3 \text{ polymer cmHg})$. The permeability $\mathcal{P} = D.S$ of CO_2 through the PAI is thus estimated as $\mathcal{P} = 10.5 \text{ cm}^3(\text{STP}) \text{ cm}/(\text{cm}^2 \text{ s cmHg}) \times 10^{-10}$, or 10.5 barrer. This compares with experimental estimates of $\mathcal{P} = 9.54$ barrer[63] and $\mathcal{P} = 15.01$ barrer[64] from the literature. The comparison between predicted and experimental values is quite favorable, given the uncertainties in the force field employed, in the structure of the model polymer, but also in the measured permeabilities.

8 Dynamic Integration of a Markovian Web and its Application to Structural Relaxation in Glasses

Glassy materials play an important role in our life and have therefore constituted an object of extensive research, both at basic and applied levels. Glasses are nonequilibrium materials, their properties depending on their formation history. Furthermore, their properties change very slowly with time in the course of "physical ageing," whose characteristic times exceed common macroscopic observation times below the glass temperature T_g. The study of glassy materials by means of molecular simulation faces serious challenges, because one needs to bridge time scales spanning some 20 orders of magnitude, from the
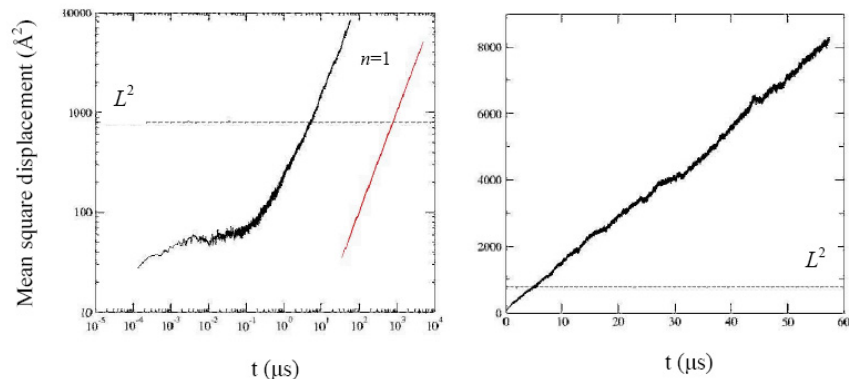
Figure 8. Mean square displacement of CO_2 penetrant in a glassy poly(amide imide) matrix as a function of time from kinetic Monte Carlo simulations of Vergadou[60] based on atomistically calculated sorption states and jump rate constants between them. (a, left): log-log coordinates; (b, right): Linear coordinates. The straight line marked $n = 1$ on the left-hand side plot indicates the expected slope for diffusion [Einstein equation, Eq. (38)]. The dotted lines labelled L^2 mark the edge length of the primary simulation cell, on which periodic boundary conditions are applied. The self- diffusivity D_s is computed from the slope of the right-hand side plot.

period of fast atomic vibrations (10^{-14} s) up to the longest time for structural, volume, and enthalpy relaxation (on the order of years $20°$ C or so below T_g).

State-of-the-art theories of the supercooled liquid state include mode coupling theory [46] and theories for enumerating stationary points [47] on the multidimensional energy hypersurface of the system. Analyses of the potential energy landscape have been reviewed. [48]

"Fragile" glass-forming liquids, whose viscosity exhibits a strongly non-Arrhenius dependence on temperature, are characterized by very rugged potential energy landscapes. This is seen characteristically in the "disconnectivity graphs" computed by D. Wales and collaborators[49] (see Figure 9). All branches of the inverted tree in a disconnectivity graph terminate at a local minimum of the energy (inherent structure). Relative energies can be read off on the vertical axis. The node (branch point) through which two inherent structures communicate corresponds to the lowest lying first-order saddle point between these structures. From the "willow tree" appearance of the graph, it is clear that there are sets of basins ("metabasins") communicating through relatively fast transitions, sets of metabasins communicating through slower transitions etc., i.e., the potential energy landscape exhibits a hierarchical structure.

The complexity of the energy landscape of a binary Lennard-Jones glass of the same composition as that studied in Ref. 49 is also seen in Figure 10, taken from the work of Tsalikis et al.[29] Here a system consisting of $N = 641$ particles is considered, at a constant number density $\rho = 1.1908\sigma_{AA}^{-3}$. To analyze the dynamics in real time units, the properties of Argon have been attributed to component A ($m_A = m_B = 6.634 \times 10^{-26}$kg, $\epsilon_{AA} = 1.65678 \times 10^{-21}$J, $\sigma_{AA} = 3.4 \times 10^{-10}$m). With these assignments, the glass temperature of the system is $T_g = 38.4K$. Figure 10 refers to a set of 290 basins that were identified as belonging to a metabasin through MD simulation at 37K. By "belonging to a metabasin" here we mean that the time required for the system to escape
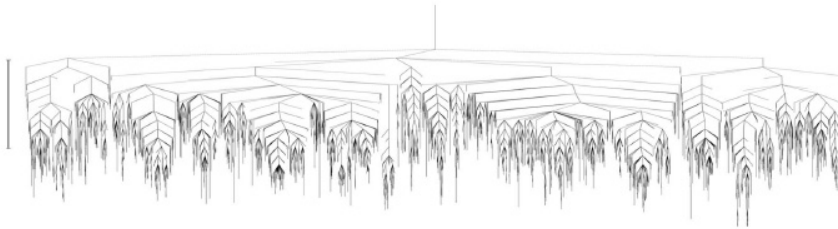
Figure 9. Disconnectivity graph for a liquid mixture of 48 A and 12 B type Lennard-Jones particles with $\epsilon_{AB} = 1.5\epsilon_{AA}$, $\epsilon_{BB} = 0.5\epsilon_{AA}$, $\sigma_{AB} = 0.8\sigma_{AA}$, $\sigma_{BB} = 0.88\sigma_{AA}$ at a particle number density $\rho = 1.3\sigma_{AA}^{-3}$, as computed from MD simulations at a temperature of 0.71 ϵ_{AA}/k_B. The glass temperature for this system is approximately $T_g = 0.32\epsilon_{AA}/k_B$. The length of the scale bar on the left corresponds to a total system energy change of 10 ϵ_{AA}.[49]

from this particular set of basins is significantly longer than the time needed for the system to establish a restricted equilibrium among the basins in the set. In a plot of the number of distinct basins visited versus time in the course of a MD simulation, this reflects itself as a plateau.[50] The number of identified distinct transitions between pairs of these 290 basins is plotted as a function of the rate constant of the transitions in Figure 10. The long-dashed line shows results from a 3 ns-long NVT MD simulation at 37 K, which was trapped within the metabasin (trajectories were turned back as soon as they were found to exit the metabasin); a total of 3910 distinct transitions were observed during this simulation. The short-dashed line shows results from a swarm of NVE MD trajectories generated in parallel off of an NVT MD trajectory at 37 K. These were able to provide a more thorough sampling of transitions within the metabasin; a total of 24271 distinct transitions were sampled. The solid line comes from a temperature-accelerated MD (TAD) method, which used as input data from swarms of NVE MD trajectories generated in parallel off of NVT MD trajectories conducted at temperatures from 37 K to 55 K. A histogram reweighting method was invoked to translate all data to 37 K (see section 3 and Ref. 29). This latter sampling method, which identified a total of 51207 distinct transitions, was able to access a rich variety of passages between the basins in the metabasin, including passages that go through high-lying terrain in the rugged potential energy landscape of the system. This explains the "wing" extending to very low rate constants on the left-hand side of Figure 10. Clearly, the fastest transitions sampled have a rate constant around $\nu_0 \simeq 10^{13}$ s^{-1}. The "nose" around 10^{10} s^{-1} is a consequence of the fact that the studied basins belong to a metabasin, so they communicate through relatively low-lying passages with each other. A time of approximately 10^{-10} s is needed for the system to visit the entire metabasin. The wing extending to very low rate constants (indeed, too low to be physically relevant at the reference temperature of 37 K, see inset) tells us something about the topography of the landscape. The inset of Figure 10 suggests a power-law distribution of rate constants between basins, of the form:

$$\rho(k_{a\to b}/\nu_0) \simeq B(k_{a\to b}/\nu_0)^{\alpha}, \quad \alpha \simeq 0.01 \tag{40}$$

and hence an exponential distribution of barrier heights $E_{a\to b} = -k_B T \ln(k_{a\to b}/\nu_0)$ Interestingly, this is similar to the form proposed for the distribution of barrier heights by J.P. Bouchaud on theoretical grounds.[51]
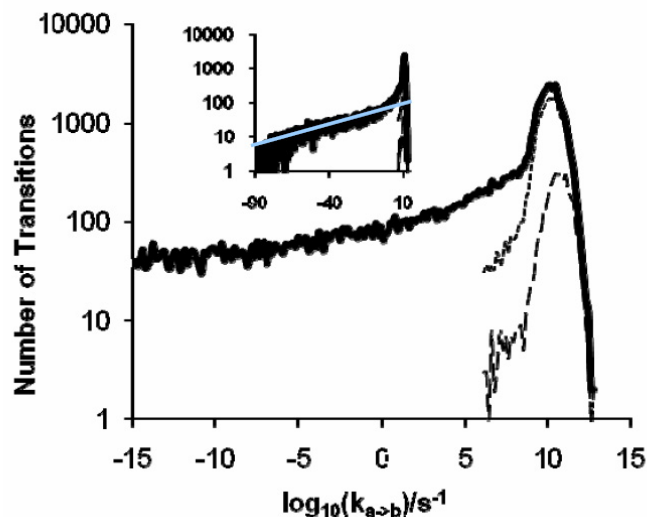
Figure 10. Number of identified distinct transitions between the 290 basins of a metabasin of a Lennard-Jones mixture at 37 K as a function of the rate constant of the transitions, as computed by three sampling methods (see text for details). The inset shows the total range of rate constants sampled by the temperature-accelerated method. The light-colored straight line through the plot in the inset corresponds to Eq. (40).

Tsalikis et al.[29] have correlated the rate constants of transitions sampled via their temperature accelerated dynamics/histogram reweighting scheme with the distance traversed in configuration space, with the cooperativity of the transitions, and with their molecular mechanisms. Fast intrabasin transitions in the binary Lennard-Jones system tend to involve single "cage-breaking" events, wherein more than half of the first neighbors of an atom change, or multiple "cage breaking" events occurring at different points in the system. Slower interbasin transitions tend to involve coordinated displacements of "chains" of atoms, wherein each atom jumps to a position close to that previously occupied by another atom in the chain. Even slower, more cooperative transitions involve extended formation of several interlinked chains or massively coordinated displacements which look like shear bands.

How do we track structural relaxation of a glass at temperatures below T_g over times relevant to the applications of glasses as structural, optical, packaging, and membrane materials? These time scales (milliseconds to years) are too long to be addressed by direct MD simulation, so reverting to an infrequent event theory-based approach seems appropriate. On the other hand, the rugged potential energy landscape of glass-forming systems gives rise to a very broad distribution of characteristic times for elementary transitions and a complex connectivity among basins. KMC simulation would have to track the fastest of these transitions, and this would limit its ability to sample long-time evolution. An approach based on analytical solution of the master equation, equivalent to averaging over all dynamical trajectories originating from a given initial distribution among basins, would seem more promising. However, it is impossible to build a complete map of all basins

and transitions between them in the rugged potential energy landscape of a glassy system even of modest size N. A way out of this difficulty is provided by the fact that, when one studies structural relaxation, one typically starts from an initial distribution among states that is highly localized (e.g. from a single basin in the potential energy landscape, where the system was trapped via the glass formation history that was followed to obtain it). The region of configuration space where the system resides is thus initially very confined, and expands gradually as transitions between basins take place.

This idea led Boulougouris and Theodorou[21] to develop a computational approach for tracking the temporal evolution of the distribution among basins (or "states") via infrequent transitions, starting off from a highly localized initial distribution, which they called "Dynamic Integration of a Markovian Web," or DIMW. DIMW distinguishes states that it samples into two categories: "explored" and "boundary" states. An "explored" state is a state for which an exhaustive calculation of as many as possible transition pathways leading out of it to neighboring states has been undertaken and rate constants associated with these transitions have been computed. In the application to isothermal - isochoric structural relaxation of a polymer glass, discussed in Ref. 21, this calculation proceeds by computing as many as possible saddle points of the potential energy in $3N - 3$-dimensional configuration space around the state under investigation using the dimer method[22] and subsequently constructing a transition path through each of these saddle points to neighboring states via Fukui's intrinsic reaction coordinate approach.[18]. Strict energy- and configuration-based criteria for identifying states that have already been visited have been implemented in connection with this exploration process.[21] For each transition pathway, a rate constant is computed. In the application presented in Ref. 21, this computation was based on transition-state theory in the harmonic approximation [compare Eq.(24)]. "Boundary" states, on the other hand, are states connected to explored states, which, however, have not been explored themselves. The DIMW algorithm proceeds as follows:

(1) All states populated according to the narrow initial distribution $\mathbf{P}(0)$ are fully explored, as described above, and boundary states connected to these states are identified. Rate constants are computed for all identified transitions emanating from an explored state and for their reverse transitions. Bookkeeping of the explored and boundary states, of the connectivity among them and of associated rate constants, is initialized. Let E and B symbolize the current set of explored and boundary states, respectively.

(2) The evolution of the occupancy probabilities of explored and boundary states for times short enough for the current set of explored states to be adequate is tracked by analytical solution of the master equation in the current explored and boundary states, initial occupancy probabilities for the boundary states being zero and all rate constants not emanating from or terminating in an explored state being taken as zero:

$$\frac{\partial P_i}{\partial t} = \sum_{j \neq i} P_j k_{j \to i} - P_i \sum_{j \neq i} k_{i \to j}, \quad i, j \in E \cup B \tag{41}$$

From the solution to Eq.(41) we compute the total probability of the system residing in the current set of explored states at time t,

$$P_E(t) = \sum_{i \in E} P_i(t). \tag{42}$$

We also compute the efflux of probability from the current set of explored states to each one of the current boundary states,

$$f_j(t) = \sum_{i \in E} P_i(t) k_{i \to j}, \quad j \in B \tag{43}$$

as well as the total efflux of probability from the current set of explored states to the current boundary states,

$$f_B(t) = \sum_{j \in B} f_j(t) \tag{44}$$

(3) For times commensurate with the first passage time for exit of the system from the current set of explored states, the latter set will no longer be adequate. Clearly, for such times the set of explored states must be augmented by including more states. We select a time t_{select} for first passage of the system out of the current set of explored states by sampling the distribution $f_B(t) / \int_0^\infty f_B(t) dt$.

(4) We pick one of the boundary states in set B, j_{select}, according to the discrete probabilities $f_j(t_{\text{select}}) / f_B(t_{\text{select}})$. The selected state will be appended to the set of explored states, E.

(5) We update the set E by including state j_{select} in it. Furthermore, we proceed to explore state j_{select} and update set B by removing state j_{select} from it and appending to it all states connected to j_{select} not already belonging to $E \cup B$ that were identified through the exploration of j_{select}. Finally, we identify a time t_{safe}, beyond which the updated sets E and B have to be used. This time is calculated via the condition $P_E(t_{\text{safe}}) = 1 - \delta$, with $P_E(t)$ being the probability of residing in the set of explored states before the update, computed in step 2. A value of $\delta = 10^{-3}$ was used in the application presented in Ref. 21.

(6) We check whether time t_{safe} has exceeded the desired simulation time. If not, we return to step 2 to solve the master equation analytically with the same initial conditions, but in the augmented set of explored states with the updated set of boundary states. For $t < t_{\text{safe}}$, the resulting solution should be practically indistinguishable from that obtained so far. For $t \geq t_{\text{safe}}$, the solution for the augmented set of explored states should be used.

As described above, DIMW amounts to a series of analytical solutions of the master equation in a set of explored and boundary states that is progressively augmented "on the fly," with rate constants determined from atomistic infrequent event analysis. The progressive augmentation of the set of explored states has a "self-healing" aspect; important connections that were missed at shorter times may be discovered as the network of explored states is expanded. The outcome from performing this calculation out to long times is a set of analytical expressions for the time-dependent probabilities $P_i(t)$ of the explored states.

Figure 11 displays the result from a DIMW calculation of structural relaxation in a 641 united atom model of glassy atactic polystyrene (aPS) at 250 K, roughly 123 K below the experimental glass temperature T_{g}, at a density of 0.951 g/cm^3, equal to the orthobaric
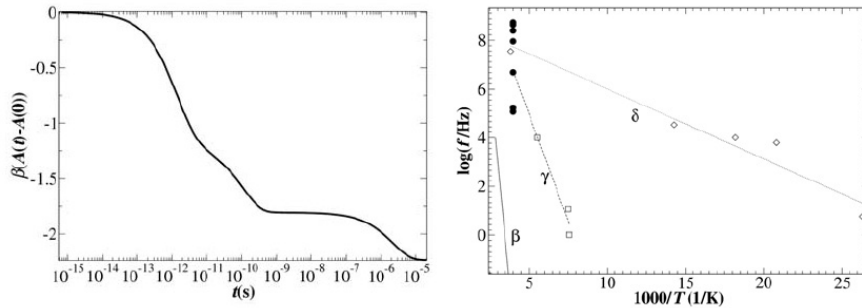
Figure 11. a (left): Helmholtz energy as a function of time for physical ageing of an aPS computer "specimen" at 250 K and initial pressure 1 bar at constant volume, as determined through the DIMW approach. b (right): Characteristic rate constants for the modes from diagonalization of the rate constant matrix at 10^{-5} s (filled symbols) compared to the peak frequencies of loss modulus measurements on aPS at various temperatures (open symbols). The quantity f on the abscissa can be identified with $-\lambda_i$ in the text.

density at that temperature.[21]. The calculation was performed out to 10^{-5} s with modest computational cost. 240 distinct states were explored and 2880 saddle points were identified in the course of the calculation. Shown in Figure 11a is a "time-dependent Helmholtz energy" for the system, calculated as

$$A(t) = \sum_i P_i(t) A_i(t) + k_\mathrm{B} T \sum_i P_i(t) \ln P_i(t), \ \ i \in E \tag{45}$$

with $P_i(t)$ being the time-dependent probability of occupancy of explored state i from the DIMW calculation and $A_i(t)$ being the Helmholtz energy of the system confined in state i, computed according to the harmonic approximation [compare Eqs. (20, 22)]. Note that $A(t)$ consists of an average of the Helmholtz energies $A_i(t)$ of the system confined in each individual state (basin), each state being weighted by its occupancy probability at time t, plus a term of entropic origin that has to do with exchange of probability among the states. At infinite time, when the system would distribute itself according to the Boltzmann distribution in its entire configuration space, $A(t)$ would become the Helmholtz energy of equilibrium thermodynamics. For the relaxing glass, which starts off occupying a single state, $A(t)$ decays with time as the system strives to approach thermodynamic equilibrium. It is interesting that this decay is not featureless, but exhibits characteristic shoulders and plateaux over specific time domains. These features betray the existence of specific relaxation processes. A plateau in $A(t)$ suggests that the system equilibrates locally within a "metabasin" of states that communicate easily with each other and is temporarily trapped there before overcoming the barriers surrounding the metabasin and moving on to states of lower free energy.

One can readily bring out the characteristic rate constants $-\lambda_i$ of modes contributing to relaxation by diagonalizing the rate constant matrix at the longest time accessed, 10^{-5} s. Results from this diagonalization are displayed in figure 11b (compare section 5). In the same figure are shown Arrhenius plots for subglass relaxation processes in aPS, determined

35
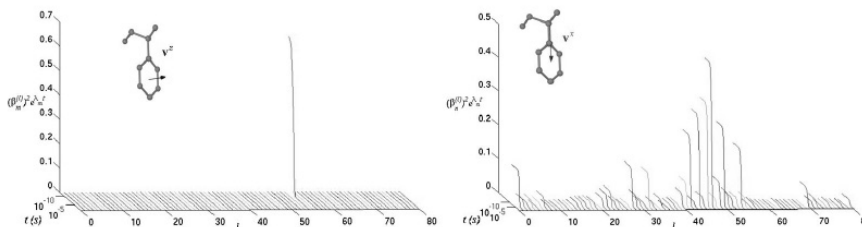
Figure 12. a (left): Fast mode ($\lambda_i = -10^{9.5} \mathrm{s}^{-1}$) contribution to the orientational decorrelation of unit vectors normal to the plane of each phenyl ring in aPS at 250 K. The index l measured along the axis running from left to right enumerates different phenyl rings in the system. b (right): Slower mode ($\lambda_i = -10^{5.2} \mathrm{s}^{-1}$) contribution to the orientational decorrelation of unit vectors along the stem of each phenyl ring in the same system.

experimentally by dynamic mechanical spectroscopy.[21] One sees that the characteristic frequencies determined by the DIMW calculation cluster in two frequency ranges, around 10^5 and around 10^9 s^{-1}. These values are quite close to the characteristic frequencies of the so-called γ and δ subglass relaxation processes determined experimentally.

Using the EROPHILE approach (Section 5), one can readily compute time autocorrelation functions for specific vectors in the system and analyze the contribution of each mode to the decay of these functions [compare Eq. (34)]. Boulougouris and Theodorou[41] have examined the autocorrelation functions of unit vectors normal to the phenyl planes and of unit vectors directed along phenyl stems. Two modes were found to contribute significantly to the decorrelation of these vectors: A fast mode with $\lambda_i = -10^{9.5} \mathrm{s}^{-1}$, which can be associated with the δ subglass relaxation process, and a slower mode with $\lambda_i = -10^{5.2} \mathrm{s}^{-1}$, which can be associated with the γ subglass relaxation process (see also Figure 11). In Figure 12, the contributions of these modes to the decorrelation of the characteristic vectors of each phenyl group l in the model glassy aPS system are displayed. The fast mode corresponds to rotation of an isolated, mobile phenyl in the system around its stem. On the other hand, the slower mode corresponds to a cooperative motion involving changes in orientation of several phenyl stems. As regards this latter motion, one can discern relatively long sequences of phenyls along the aPS chain that exhibit very little decorrelation. These sequences tend to be syndiotactic in their stereochemical configuration.

This aPS example shows how mechanictic aspects of dynamics in a system with very complex potential energy landscape can be explored in an unbiased way using a combination of DIMW and EROPHILE methodologies.

9 Lumping

A difficulty with DIMW-type approaches (see Section 8) is that the number of states to be tracked becomes prohibitively large at long times. A way out of this problem is to group, or "lump," states communicating via transitions that are fast in relation to the observation time into single clusters of states. If performed judiciously, this lumping does not result in loss of essential information. At long observation times, the system distributes itself

among fast-communicating states according to the requirements of a restricted equilibrium (compare plateaux in Figure 11a), so clusters of such states behave as single "meta-states," for all practical purposes.

From the mathematical point of view, lumping is not a new problem. It has been examined in the context of networks of chemical reactions in the classic work of Wei and Kuo [52] and in several subsequent works. As shown there, lumping calls for the determination of a $\hat{n} \times n$ transformation matrix $\mathbf{M}$, where n is the number of original states and $\hat{n} < n$ is the number of lumped states (or clusters of states). The transformation from the probability distribution among the original states to that among the lumped states at any time t takes place according to the equation

$$\hat{\mathbf{P}}(t) = \mathbf{M} \cdot \mathbf{P}(t) \tag{46}$$

The lumping matrix $\mathbf{M}$ has the following properties:

i. The elements of matrix $\mathbf{M}$ are either "0" or "1".

ii. Every column of matrix $\mathbf{M}$ contains exactly one "1". The physical meaning behind this is that every state of the original description (assigned to a column of $\mathbf{M}$) belongs to one cluster only (assigned to a row of $\mathbf{M}$).

iii. The position of "1" in every column of $\mathbf{M}$ (i.e., state in the original description) describes to which cluster (row of $\mathbf{M}$) the state of the initial system is being lumped.

Once $\mathbf{M}$ is known, the $\hat{n} \times \hat{n}$ rate constant matrix $\hat{\mathbf{K}}$ to be used at the lumped level is calculated as

$$\hat{\mathbf{K}} = \mathbf{M} \cdot \mathbf{K} \cdot \mathbf{A} \cdot \mathbf{M}^{\mathrm{T}} \cdot \hat{\mathbf{A}}^{-1} \tag{47}$$

where $\mathbf{A}$ is a $n \times n$ diagonal matrix whose diagonal elements equal the elements of the equilibrium probability vector $\mathbf{P}(\infty)$ corresponding to the original rate constant matrix $\mathbf{K}$, the superscripts "T" and "-1" indicate matrix transpose and matrix inverse, respectively, and

$$\hat{\mathbf{A}} = \mathbf{M} \cdot \mathbf{A} \cdot \mathbf{M}^{\mathrm{T}} \tag{48}$$

Lempesis et al.[43] proposed a methodology for the determination of the number of lumped states $\hat{n}$ and the lumping matrix $\mathbf{M}$ in such a way that the long-time dynamics of the original description is reproduced. The strategy is to minimize an objective function of the form

$$z(\hat{n}, \mathbf{M}) = z_1 E + z_2 W + z_3 \hat{n} \tag{49}$$

with z_1, z_2, z_3 being pre-defined real positive constants.

E is the Frobenius norm of the $\hat{n} \times n$ error matrix $\mathbf{E}$:[52]

$$E = ||\mathbf{E}||_F = \sqrt{\sum_{i=1}^{\hat{n}} \sum_{j=1}^{n} |E_{ij}|^2} \tag{50}$$

$$\mathbf{E} = \mathbf{M} \cdot \mathbf{K} - \hat{\mathbf{K}} \cdot \mathbf{M} \tag{51}$$

For exact lumping, the lumping error E would be zero. W, on the other hand, is the Frobenius norm of the lumped matrix $\hat{\mathbf{K}}$:

$$W = ||\hat{\mathbf{K}}||_F = \sqrt{\sum_{i=1}^{\hat{n}} \sum_{j=1}^{\hat{n}} |\hat{K}_{ij}|^2} \tag{52}$$

Including a term proportional to W in the objective function, Eq. (49), forces the minimization to focus on long times (small W) in matching the dynamics between the original and the lumped system. Including a term proportional to $\hat{n}$ in the objective function, on the other hand, encourages the algorithm to keep the dimensionality of the lumped system as small as possible.

The minimization of the objective function defined in Eq. (49) is performed stochastically, using Monte Carlo moves which change the dimensionality $\hat{n}$ and the form of the lumping matrix $\mathbf{M}$, while respecting the constraints on the form of that matrix stated above. To avoid trapping in local minima of the objective function, a Wang-Landau scheme is invoked to determine the density of $\mathbf{M}$-matrix "states" in the space of variables $(E, W, \hat{n})$ and pick that $\mathbf{M}$, close to the origin of $(E, W, \hat{n})$ space, which minimizes the objective function.[43]

Figure 13 shows results from application of the lumping strategy of Lempesis et al.[43] to a mixture of 641 Lennard-Jones particles with the interaction parameters stated in section 8 and atomic fractions 80% A, 20% B, at a temperature of 37 K, just below T_{g}. Shown are histograms of the negative inverse eigenvalues $t_i = -1/\lambda_i$ of the rate constant matrices $\mathbf{K}$ (original description) and $\hat{\mathbf{K}}$ (lumped description). The overall shapes of the histograms are seen to be similar. Furthermore, the eight longest t_i values are seen to agree quantitatively between the original and lumped system, testifying to the success of the lumping method in reproducing the long-time dynamics of the original system.

10 Summary

Addressing long-time ($> 1\mu$s) dynamics in many materials, complex fluid, and biomolecular systems constitutes a great challenge for molecular simulations. In many cases, the temporal evolution of a system is slow because the system spends a long time confined within regions in configuration space ("states") and only infrequently jumps from state to state by overcoming a (free) energy barrier separating the states. We have briefly discussed ways of probing the time scale separation underlying these infrequent transitions and identifying states, either in terms of all the degrees of freedom or in terms of appropriately chosen slow variables or order parameters. We have also reviewed analytical and simulation techniques, based on the theory of infrequent events, for estimating the rate constants $k_{i \rightarrow j}$ for transitions between states.

Emphasis in these notes has been placed on how we predict the long-time dynamical evolution once we have identified a network of states and computed the rate constants between them. We have discussed the principles of two categories of methods for doing this:
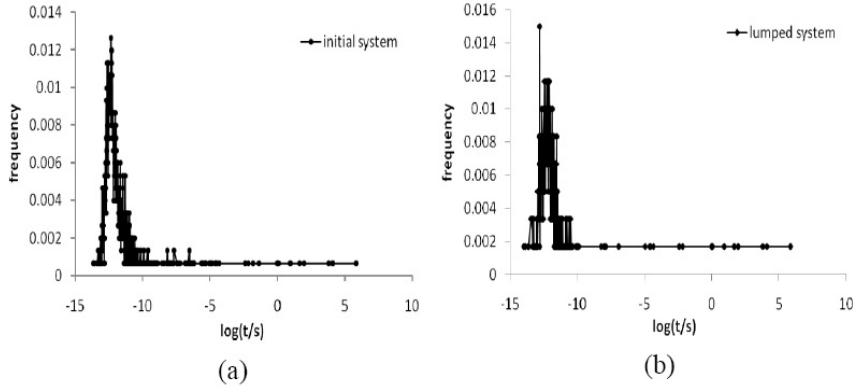
Figure 13. Histogram of the negative inverse eigenvalues for (a) the initial description, (b) the lumped description of the dynamics of a mixture of 641 Lennard-Jones particles just below T_g (see text for details). There are $n = 1502$ eigenvalues in (a) and $\hat{n} = 600$ eigenvalues in (b).

Kinetic Monte Carlo simulations, which generate long stochastic trajectories for the evolution of the system; and analytical solution of the master equation, which yields expressions for the time-dependent probabilities of occupancy of the states as sums of exponentially decaying functions after diagonalization of an appropriately symmetrized rate constant matrix. We have seen that the analytical solution to the master equation can form the basis for calculating useful time-dependent ensemble averages and correlation functions that quantify the approach to equilibrium and enable the calculation of time-dependent properties in the context of the Eigenvalue Representation of Observables and Probabilities in a HIgh-dimensional Euclidean space[41] (EROPHILE) approach. We have presented applications of both Kinetic Monte Carlo and analytical solution of the master equation to problems of diffusion in zeolites and in amorphous polymers. We have also discussed advantages of the analytical solution in cases where the spectrum of characteristic times for evolution on the network of states, quantified by the eigenvalues of the rate constant matrix, is very broad. In systems characterized by spatial periodicity, such as zeolites, analytical solution of the master equation can be made several orders of magnitude faster than Kinetic Monte Carlo, thanks to a recursive scheme[44] (MESoRReD) that reduces diagonalization of the rate constant matrix for the whole system to diagonalization of much smaller matrices pertaining to a single unit cell.

Nonequilibrium systems with rugged or fractal potential energy hypersurfaces, such as glasses, preclude the a priori determination of all states and transitions between them. One is often interested in the evolution of such systems starting from a narrow, localized distribution in configuration space (e.g., tracking the structural relaxation of a glassy configuration). For addressing this problem, we have introduced Dynamic Integration of a Markovian Web[21] (DIMW), which solves the master equation in a network of states that is progressively augmented as time elapses based on an "on the fly" exploration of configuration space and calculation of rate constants. Application of the DIMW approach to

a polymer glass has yielded promising results. To keep the number of states manageable at long times, DIMW can be complemented by a "lumping" algorithm[43] which groups fast-communicating states into single "metastates." This algorithm has been applied successfully to a glassy binary Lennard-Jones mixture.

It is hoped that the concepts and computational tools discussed here may be useful in addressing the long-time properties of systems enountered in the wide range of problems addressed by today's physicists, chemists, chemical engineers, materials scientists, and molecular biologists, starting from fundamental atomic-level information.

11 Acknowledgments

References

1. G. H. Vineyard, *Frequency factors and isotope effects in solid state rate processes*, J. Phys. Chem. Solids **3**, 121–127, 1957.

2. A. A. Gusev, F. Móller-Plathe, W. F. van Gunsteren, U. W. Suter, *Dynamics of small molecules in bulk polymers*, Advan. Polym. Sci. **116**,207-247, 1994.

3. D. N. Theodorou, R. Q. Snurr, A. T. Bell, *Molecular dynamics and diffusion in microporous materials*, in G. Alberti, T. Bein (Eds.) *Comprehensive Supramolecular Chemistry* (Elsevier Science, Oxford, 1994), pp 507-548.

4. F. H. Stillinger, *A topographic view of supercooled liquids and glass formation*, Science **267**, 1935-1939, 1995.

5. D. J. Wales, J. P. K. Doye, M. A. Miller, P. N. Mortenson, T. R. Walsh, *Energy landscapes: from clusters to biomolecules*, Advan. Chem. Phys. **115**, 1-111,2000.

6. A. F. Voter, J. D. Doll, *Dynamical corrections to transition-state theoryfor multistate systems - Surface self-diffusion in the rare event regime*, J. Chem. Phys. **82**, 80-92, 1985.

7. P. G. Wolynes, *Energy landscapes and solved protein-folding problems* Phil. Trans. Roy. Soc.A **363**,453-464,2005.

8. J. Wei, C. D. Prater, *The structure and analysis of complex reaction systems*, Advan. Catal. **13**,204-390, 1962.

9. D. E. Shaw, *Millisecond-long molecular dynamics simulations ofproteins on the Anton machine*, in *Proceedings of FOMMS 2009: Foundations for Innovation*, Blaine, WA, 2009.

10. D. Chandler, *Statistical-mechanics of isomerization dynamics in liquids and transition-state approximation* J. Chem. Phys. **68**,2959-2970, 1978.

11. D. Chandler, *Throwing ropes over rough mountain passes, in the dark* in B. J. Berne, G. Ciccotti, D. F. Coker (Eds.) *Classical and quantum dynamics in condensed-*

phase simulations (World Scientific, Singapore, 1998), pp 55-66.

12. W. Feller, *An introduction to probability theory and its applications: Volume 2* (John Wiley, New York, 1971).

13. R. L. June, A. T. Bell, D. N. Theodorou, *Transition state studies of xenon and SF_6 diffusion in silicalite* J. Phys. Chem. **95**, 8866-8878, 1991.

14. R. Q. Snurr, A. T. Bell, D. N. Theodorou, *Investigation of the dynamics of benzene in silicalite using transition-state theory* J. Phys. Chem. **98**, 11948-11961, 1991.

15. M. L. Greenfield, D. N. Theodorou, *Molecular modeling of methane diffusion in glassy atactic polypropylene via multidimensional transition state theory* Macro-molecules **31**, 7068-7090, 1998.

16. M. L. Greenfield, D. N. Theodorou, *Geometric analysis of diffusion pathways in glassy and melt atactic polypropylene* Macromolecules **26**, 5461-5472, 1993.

17. J. Baker *An algorithm for the location of transition states* J. Comput. Chem **7**, 385-395, 1986.

18. K. Fukui, *The path of chemical reactions - the IRC approach* Acc. Chem. Res. **14**, 363-368, 1981.

19. D. N. Theodorou, *Principles of molecular simulation ofgas transport in polymers*, in Y. Yampolskii, I. Pinnau, B. Freeman (Eds.) *Materials Science ofMembranesfor Gas and Vapor Separation* (John Wiley and Sons, New York, 2006), pp 49-94.

20. N. P. Kopsias, D. N. Theodorou, *Elementary structural transitions in the amorphous Lennard-Jones solid using multidimensional transition-state theory* J. Chem. Phys. **109**, 8573-8582, 1998.

21. G. C. Boulougouris, D. N. Theodorou, *Dynamical integration of a Markovian web: a first passage time approach* J. Chem. Phys. **125**, 084903,2007.

22. G. Henkelman, H. Jσnsson, *A dimer methodfor finding saddle points in high dimensional potential surfaces using only first derivatives* J. Chem. Phys. **111**, 7010-7022, 1999.

23. T. R. Forester, W. Smith, *Bluemoon simulations of benzene in silicalite-1: Prediction offree energies and diffusion coefficients* J. Chem. Soc., Faraday Trans. **93**, 3249-3257, 1997.

24. D. Frenkel, B. Smit, *Understanding molecular simulation: From algorithms to applications*, 2nd Edition, (Academic Press, New York, 2002).

25. F. H. Stillinger, T. A. Weber, *Hidden structure in liquids* Phys. Rev. A **25**, 978-989, 1982.

26. E. Helfand, *Brownian dynamics study of transitions in a polymer chain of bistable oscillators* J. Chem. Phys. **69**, 1010-1018, 1978.

27. D. G. Tsalikis, N. Lempesis, G. C. Boulougouris, D. N. Theodorou, *On the role of inherent structures in glass forming materials: I. The vitrification process* J. Phys. Chem. B **112**, 10619-10627, 2008.

28. M. R. Sψrensen, A. F. Voter *Temperature-accelerated dynamics for simulation of infrequent events* J. Chem. Phys. **112**, 9599-9606,2000.

29. D. G. Tsalikis, N. Lempesis, G. C. Boulougouris, D. N. Theodorou, *Temperature accelerated dynamics in glass-forming materials* J. Phys. Chem. B **114**, 7844-8753, 2010.

30. C. H. Bennett, *Exact defect calculations in model substances* in A. S. Nowick, J. J. Burton (Eds.) *Diffusion in solids: recent developments* (Academic Press: New York, 1975),pp 73-113.

31. M. P. Allen, D. J. Tildesley, *Computer simulation of liquids* (Clarendon, Oxford, 1987).

32. D. A. Kofke, *Free energy methods in molecular simulation* Fluid Phase Equil. **228**, 41-48,2005.

33. P. Yi and G. C. Rutledge, *Molecular origins of homogeneous crystal nucleation* Annu. Rev. Chem. Biomol. Eng. **3**, in press, 2005.

34. S. Singh, C. C. Chiu, J. de Pablo *Flux Tempered Metadynamics* J. Stat. Phys. **144**, 1-14, 2011.

35. A. Laio, M. Parrinello *Escaping free energy minima* Proc. Natl. Acad. Sci. USA **99**, 12562-125 66, 2002.

36. P. G. Bolhuis, D. Chandler, C. Dellago, P.L. Geissler *Transition Path Sampling: Throwing ropes over mountain passes, in the dark* Annu. Rev. Phys. Chem. **53**, 291-3 18, 2002.

37. C. Dellago, P. G. Bolhuis, P. Geissler *Transition Path Sampling* Adv. Chem. Phys. **123**, 1-78, 2002.

38. A. F. Voter, *Introduction to the Kinetic Monte Carlo Method* in K. E. Sickafus, E. A. Kotomin, B. P. Uberuaga (Eds.), *Radiation Effects in Solids*, NATO Science Series II: Mathematics, Physics, and Chemistry, Vol. 235 (Springer: Dordrecht, The Netherlands, 2007), Chapter 1, pp 1-23.

39. D. E. Knuth, *The art of computer programming* Vol.2, (Addison-Wesley, Reading, MA, 1997), Chapter 3.

40. N. V. Buchete and G.Hummer, *Coarse master equations for peptide folding dynamics*, J. Phys. Chem. B **112**, 6057-6069,2008

41. G. Boulougouris, D. N. Theodorou, *Probing subglass relaxation in polymers via a geometric representation of probabilities, observables, and relaxation modes for discrete stochastic systems* J. Chem. Phys. **130**, 044905,2009.

42. K. E. Shuler, *Relaxation processes in multistate systems* Phys. Fluids **2**, 442-448, 1959

43. N. Lempesis, D. G. Tsalikis, G. C. Boulougouris, D. N. Theodorou, *Lumping analysis for the prediction of long-time dynamics: From monomolecular reaction systems to inherent structure dynamics of glassy materials* J. Chem. Phys. **135**,204507,2011.

44. P. Kolokathis, D. N. Theodorou, *On solving the master equation in spatially periodic systems*, in preparation

45. R. L. June, A. T. Bell, D. N. Theodorou, *Molecular dynamics study of methane and xenon in silicalite* J. Phys. Chem **94**, 8232-8240, 1990

46. Gφtze, W., *Aspects of structural glass transitions*, in J.P. Hansen, D. Levesque, J. Zinn-Justin (Eds.) *Les Houches Session LI, 1989 Liquids, Freezing and Glass Transition* (Elsevier Science Publishers B.V., Amsterdam 1991), pp 287-503.

47. S. M. Shell, P. G. Debenedetti, A. Z. Panagiotopoulos *A conformal solution theory for the energy landscape and glass transition of mixtures* Fluid Phase Equilib. **241**, 147-154,2006.

48. F. Sciortino, *Potential energy description of supercooled liquids and glasses* J. Stat. Mech. , P0505 15, 2005

49. V. K. de Souza, D. J. Wales, *Connectivity in the potential energy landscape for binary Lennard-Jones systems* J. Chem. Phys. **130**, 194508,2009

50. D. G. Tsalikis, N. Lempesis, G. Boulougouris, D. N. Theodorou, *Efficient parallel decomposition of dynamical sampling in glass-forming materials based on an "on the fly" definition of metabasins* J. Chem. Theory Comp. **6**, 1307-1322,2010

51. J. P. Bouchaud, *Weak ergodicity breaking and aging in disordered systems* J. Phys. I France **2**, 1705-1713, 1992

52. J. Wei, J. C. W. Kuo, *A lumping analysis in monomolecular reaction systems - Analysis of exactly lumpable systems* Ind. Eng. Chem. Fundam. **8**, 114-123, 1969

53. J. Kδrger, H. Pfeifer, F. Stallmach, N. N. Feoktistova, S.P. Zhdanov, ^{129}Xe *and* $13C$ *PFG-NMR study of the intracrystalline self- diffusion of Xe, CO2, and CO* Zeolites **13**, 50-55, 1993

54. H. G. Karge, J. Weitkamp, *Molecular sieves - Characterization II* (Springer, Berlin, 2007)

55. D. N. Theodorou, *Hierarchical modelling ofpolymeric materials* Chem. Eng. Sci. **62**, 5697-57 14, 2007

56. A. A. Gusev, U. W. Suter, *Dynamics ofsmall molecules in polymers subject to thermal motion* J. Chem. Phys. **99**,2228-2234, 1993

57. A. A. Gusev, U. W. Suter, W. R. van Gunsteren, U. W. Suter, *Dynamics of small molecules in bulk polymers* Advan. Polym. Sci. **116**,207-247, 1994

58. M. L. Greenfield, D. N. Theodorou, *Coarse-grained molecular simulation ofpenetrant diffusion in a glassy polymer using reverse and Kinetic Monte Carlo* Macromolecules **34**, 8541-8553,2001

59. M. L. Greenfield, *Sorption and diffusion of small molecules using Transition State Theory* in M. J. Kotelyanskii and D. N. Theodorou (Eds.) *Simulation methods for polymers* (Marcel Dekker, New York 2004)

60. N. Vergadou, *Prediction of gas permeability of stiff-chain amorphous polymers through molecular simulation methods* (Ph.D. Thesis, Chemistry Department, University of Athens, 2006)

61. N. Ch. Karayiannis, V. G. Mavrantzas, D. N. Theodorou, *Diffusion ofsmall molecules in disordered media: study of the effect of kinetic and spatial heterogeneities* Chem. Eng. Sci. **56**,2789-2801,2001

62. L. Garrido, M. Lσpez-Gonzαlez, E. Riande, *Influence of local chain dynamics on diffusion ofgases in polymers as determined bypulsedfield gradient NMR* J. Polym. Sci. B: Polym. Phys **48**,231-235,2010

63. D. Fritsch, K. V. Peinemann, *Novel permeselective 6F-poly(amide imide)s as membrane hostfor nano-sized catalysts* J. Membr. Sci. **99**, 29-38, 1995

64. C. Nagel, K. Gunther-Schade, D. Fritch, T. Strunskus, F. Faupel, *Free volume and transport properties in highly selective polymer membranes* Macromolecules **35**, 2071-2077,2002